FABRICATION OF TCO-LESS DYE-SENSITIZED SOLAR CELLS

PhD DISSERTATION

OHNMAR SOE

DEPARTMENT OF PHYSICS
UNIVERSITY OF YANGON
MYANMAR

MAY 2014

FABRICATION OF TCO-LESS
DYE-SENSITIZED SOLAR CELLS

OHNMAR SOE

THIS DISSERTATION IS SUBMITTED TO THE BOARD OF EXAMINERS IN PHYSICS, UNIVERSITYOF YANGON FOR THE DEGREE OF DOCTOR OF PHILOSOPHY

EXTERNAL EXAMINER
Dr Myint Kyi
Pro-Rector (Rtd.)
ITBMU

CHAIRPERSON
Dr Khin Mar Kyu
Professor and Head
Department of Physics
University of Yangon

REFEREE
Dr Aye Thein
Associate Professor (Rtd.)
Department of Physics
Dagon University

MEMBER
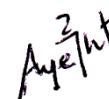Dr Nwe Ni Khin
Professor
Department of Physics
University of Yangon

MEMBER
Dr Khin Hlaing
Associate Professor
Department of Physics
University ofYangon

SUPERVISOR
Dr Pho Kaung
Pro-Rector
Universities' Research Centre
University of Yangon

CO-SUPERVISOR
Dr Aye Aye Thant
Associate Professor
Department of Physics
University of Yangon

CONTENTS

Page

REFERENCES

ACKNOWLEDGEMENTS

ABSTRACT

The technology of the dye-sensitized solar cells (DSSCs) was studied theoretically. It was found that using two transparent conductive oxide layer (TCO) in both electrodes of DSSCs takes more costs. The nanoporous fluorine doped tin oxide, F: SnO_2 powder has been prepared for the fabrication of low cost DSSCs. In this research, all DSSCs have been fabricated without commercial TCO glasses. The carbon enrich counter electrodes have been used for donation and acceptance of electrons for oxidized dye molecules and reduced electrolyte ions. To enhance the current collection, FTO electrodes have been made and applied in DSSCs' fabrication. X-ray diffraction analysis confirmed the prepared (F: SnO_2) nanocrystallite powder has single phase of tetragonal rutile structure. Scanning electron microscopy (SEM) shows porous structure of (F: SnO_2) powder for dye adsorption. The sol–gel combustion method offers a simple and effective route for the synthesis of nanoporous F:SnO_2 materials. The working electrodes of DSSCs have been prepared by fluorine doped tin oxide powder. The various counter electrodes have been used to study the working principles and to measure current-voltage characteristic of TCO-less DSSCs. The fill factor (FF) and efficiency (η) of these cells have also been calculated from I-V characteristic curve of fabricated DSSCs. F :SnO_2 based TCO-less DSSCs sample without metal mesh has η of about 0.03% with FF of 0.44, open circuit voltage (V_{oc}) of 0.56 V and short circuit current (I_{sc}) of 0.11 mA and that of with metal mesh has η of 0.1092% ,FF of 0.48, V_{oc} of 0.56 V and I_{sc} of 0.38 mA.

LIST OF FIGURES

LIST OF TABLES

REFERENCES

1. Alex B F 2005 "New Architectures for Dye-Sensitized Solar Cells" (New York: Willey).

2. Brinker C J and Scherer G W 1990 "Sol-Gel,Science The Physics and Chemistry of sol-gel Processing" (New York: Academic Press).

3. Gratzel M 2000 "Perspectives for dye-sensitized nanocrystalline solar cells. Prog. Photovolt" : Res Appl.8 171

4. Richard Rivera Freddy Marcillo Alexander Chamba Patricio Puchaicela and Arvids Stashans 2014 "Quantum Chemical Study of Point Defects in Tin Dioxide" (Springer Science+Business Media Dordrecht)

5. Robertson J and Falabrett B 2010 "Electronic Structure of Transparent Conducting Oxides" (Springer Science + Business Media Cambridge)

6. Paul A Lynn 2010 "Electricity from Sunlight: An Introduction to Photovoltaic's" (New York: Willey).

7. Sandra E Dann 2000 "Reactions and Characterization of Solids", (Cambridge: The Royal Society of Chemistry).

8. Suryanarayana C & Grant Norton M 1956 "X-Ray Diffraction, A practical Approach" (New York: Plenum Press).

9. http://www.springer.com

10. http://www.sciencedirect.com

11. http://www.opticsinfobase,org

12. http://www.osti.gov/bridge

13. http://www.gigapedia.com

<p style="text-align:center">Referee's Report</p>

Candidate :   Ohnmar Soe
Roll No.   :   4 PhD-Phys-3
Thesis Title :   Fabrication of TCO-Less Dye-Sensitized Solar Cells

Ohnmar Soe's doctoral research work involved the fabrication of Dye-Sensitized Solar Cells (DSSCs), improving the technology of nanoporous Fluorine doped Tin Oxide powder (nc-F:SnO_2) to replace the expensive Transparent Conductive Oxide (TCO) electrode in DSSC. F:SnO_2 powder was prepared by auto-combustion assisted sol-gel method. $SnCl_4$ and HF were dissolved in deionized water with acetylene black. The gel was heated up to 750ºC. The color of the powder is white. The XRD studies of F:SnO_2 powder indicated the tetragonal rutile structure and SEM image proved the typical porous pores existence.

To get FTO electrode, the glass substrates were coated by two techniques; spin coating and Spray Pyrolysis deposition (SPD) techniques. UV-Vis spectroscopy shows all the FTO films have good transmittance in visible region. Two point probes method has shown that these films has lower resistance and can be used as n-type electrode in the fabrication of DSSCs. The results for photovoltaic properties are credible. In TCO-less DSSC the energy conversion efficiency is low, but fill factor is high.

The outcomes of her research are applicable in developing photo-chemical solar cells. The objectives of the research are clear and appropriate. The candidate has done well in an original research work. The candidate is fully recommended for the PhD degree in Physics.

May 6,2014

Dr Aye Thein
Accociate Professor (Rtd.)
Department of Physics
Dagon University

External Examiner's Report

Candidate : Ohnmar Soe

Roll No.   : 4 PhD-Phys-3

Thesis Title : Fabrication of TCO-Less Dye-Sensitized Solar Cells

A new type of dye-sensitized solar cell (DSSC) based on nanoporous ($F:SnO_2$) electrode without TCO layer is fabricated by sol-gel combustion method for low-cost solar cell.

The prepared ($F:SnO_2$) nano crystalline powder were characterized by XRD, SEM and UV-Vis spectroscope. Results show that fluorine doped tin oxide powder can be used for TCO-less dye-sensitized solar cells' fabrication.

We examine the candidate for just over two hours, satisfying overselves that the work reported in the thesis was indeed her own and the thesis has been written by her. The candidate demonstrated an excellent grasp of her research area and associated areas. The candidate was able to engage with the examiners in detailed and technical debate about all aspect of the work. The candidate defended the thesis very well at the viva.

I have no hesitation in recommendation the award of the PhD degree.

May 6, 2014

Professor Dr Myint Kyi

Pro-Rector (Rtd.)

ITBMU

CHAPTER I

INTRODUCTION

In the previous century, it is obvious that the consumption of nonrenewable sources of energy has caused more environmental damage than any other human activity. Energy generated from fossil fuels has led to face many problems such as exhaustion of fossil fuels, ozone depletion, global warming, climate change and social and political risks. Therefore, renewable source of energy such as Hydropower, Wind, Solar, Biomass, Geothermal and others have become very important and relevant to today's world.

Solar photovoltaic cells have a promising form of renewable energy. A solar cell is a photonic device that converts photons with specific wavelengths to electricity. First and second generations photovoltaic cells are mainly constructed from semiconductors including crystalline silicon, III-V compounds, cadmium telluride, and copper indium selenide/sulfide. The primary obstacle to the broader uptake of solar photovoltaic technology is the manufacturing cost of current commercial solar cells. Low cost solar cells have been the subject of intensive research work for the last three decades. Amorphous semiconductors were announced as one of the most promising materials for low cost energy production.

Thin Dye-sensitized solar cells, or DSSCs, are a third generation technology in the area of photovoltaic's. They are classified as a type of thin-film solar cell, meaning that they require only a small amount of material per cell compared to the first generation solar cells, making DSSCs lighter and more physically resilient than their first generation counterparts. They use a process similar to photosynthesis to produce electrical energy, making them an example of biomimicry. Michael Gratzel and coworkers at the Ecole Polytechnique Federale de Lausanne (Gratzel, 2003; Nazerruddin et al., 1993; O' Regan& Gratzel, 1991) succeeded for the first time to produce what is known as

"Gratzel Cell" or the DSSC to imitate photosynthesis (the natural processes plants convert sunlight into energy) by sensitizing a nanocrystalline TiO_2 film using novel Ru bipyridl complex.

General comparison between semiconductor based solar cells and DSSCs is presented in Table 1.1. Incorporation of dye molecules in some wide band gap semiconductor electrodes was a key factor in developing photoelecrochemical solar cells.

Since DSSCs are inexpensive and resilient, they are ideal for large scale and small scale applications. However, they have lower efficiencies than most other types of solar cells, so they require more space than other types of solar cells to produce the same amount of electric energy. This disadvantage is offset by their low cost and greater resilience and flexibility.

In all DSSCs fabrication; the cost of TCO takes 60% of cells' fabrication cost. Therefore, in this research, to reduce this cost, nanocrystaliine fluorine doped tin oxide (nc-F:SnO_2)powder is used in the place of TCO glass and TiO_2 powder. To enhance the current collection, FTO electrodes have been made and applied in DSSCs' fabrication.

Table 1.1. Comparison between semiconductors based solar cells and the Dye Sensitized Solar Cells (DSSCs).

Quality	Semiconductor solar cells	Dye Sensitized Solar Cells

Transparency	Opaque	Transparent
Pro-Environment (Material &Process)	Normal	Great
Power Generation Cost	High	Low
Power Generation Efficiency	High	Normal
Color	Limited	Various

CHAPTER II

BACKGROUND KNOWLEDGE

2.1 The Solar Energy and Solar Cells

Solar Energy is the energy obtained from the sun. It's the most efficient and clean source of energy to drive the latest trends in the market. Solar energy in the form of photovoltaic cells (PV) has been extensively used in electricity and the related areas.

The intensity of solar radiation in the earth's distance from the sun is approximately 1353 kW/m^2, a number also called *the solar constant*. The solar radiation is emitted from the sun's photosphere at 6000 K temperature, which gives it a spectral distribution resembling closely that of a black body at the corresponding temperature. Passing through the earth's atmosphere the solar radiation is attenuated by scattering from the air molecules, aerosols and dust particles, as well as by absorption by the air molecules, in particular oxygen, ozone, water vapor, and carbon dioxide. This gives a characteristic fingerprint to the solar radiation spectrum on the earth's surface as shown in Figure 2.1. The path length in units of Air Mass, change with the zenith angle is shown in Figure 2.2.

The smooth curve in Figure 2.1 shows that such black - body radiation spreads over wavelengths between about 0.2 and 2.0 μ m, with a peak around 0.5 μ m. The range of wavelengths visible to the human eye is about 0.4 μ m (violet) to 0.8 μ m (red). Shorter wavelengths are classed as ultraviolet (UV), longer ones as infrared (IR). Note how much of the total spectrum lies in the IR region. The figure shows two more curves, labeled AM0 and AM1.5, representing actual solar spectral distributions arriving at Earth. To explain these we need to consider the path length or Air Mass (AM) of sunlight through the atmosphere. AM0 refers to sunlight just outside the atmosphere (path length zero) and is therefore relevant to (PV) used on Earth satellites. In the case of terrestrial PV, the path length is the same as the thickness of the atmosphere (AM1) when the Sun is directly overhead. But if it is not overhead the path length increases according to an inverse cosine law. For example when 60 ° from overhead the path length is doubled (AM2), and so on. The overhead and is generally

accepted as a compromise for assessing PV cells and systems. The deep notches are due to absorption by oxygen, water vapors, and carbon dioxide.

Solar electricity is a steadily growing energy technology today and solar cells have found markets in variety of applications ranging from consumer electronics and small scale distributed power systems to centralized megawatt scale power plants. Direct utilization of solar radiation to produce electricity is close to an ideal way to utilize the nature's renewable energy flow.

2.2. Development of Solar Cells

Solar cells, or photovoltaic (PV) cells, are electrical devices that directly convert sunlight into electricity. Since the modern discovery of the silicon p-n junction PV devices (solar cells) in the early 1950s, the global PV industry has experienced revolutionary developments and market growth. The solar industry has been the fastest growing renewable energy technology in recent years.

The first generation of solar cells from industrialization point of view is based on crystalline silicon. This type of solar cells is currently dominant in the PV market due to the high efficiency of up to 25%. However, the manufacture of silicon-based solar cells involves high purity silicon, the manufacturing processes of which are extremely expensive. The silicon-based PV industry relies heavily on government subsidies so far. The high cost of the first generation solar cells severely restricts their widespread application in the future.

The second generation of solar cells is normally referred to as thin-film solar cells. Amorphous silicon, cadmium telluride (CdTe) and copper indium gallium selenide (CIGS) are the three most commonly used materials for the second generation solar cells. The thin-film technology allows the second generation solar cells to use far less materials required in a solar cell, which significantly reduce the production cost in contrast to the first generation solar cells. However, the efficiencies of thin-film solar cells are lower than the first

generation solar cells, ranging between 10-20%. Moreover, the scarcity and toxicity of the materials being used have been two major disadvantages for thin-film solar cells from a large-scale production point of view.

Dye-sensitized solar cells (DSSCs), also known as Grätzel cells, were significantly improved in 1991 by Brian O'Regan and Michael Grätzel at the École Polytechnique Fédérale de Lausanne in Switzerland. In contrast to conventional systems where the semiconductor takes both the function of light absorption and charge carrier transport; these two functions are separated in DSSCs. The light absorption is performed by a monolayer of dye molecules attached to a mesoporous layer of a wide band gap semiconductor. Charge separation takes place at the semiconductor/dye interface. Charge carriers are transported in the conduction band edge (CB) of the semiconductor to the charge collector.

DSSCs are considered to be a technology between the second and third generation solar cells. The record efficiencies of DSSCs have shown up to 12% in small cells, and 10% in sub-modules. Of particular interest is the low production cost for the fabrication of a DSSC. The materials used in DSSCs are inexpensive, for instance, the commonly used semiconductor, titanium, is very cheap and is widely used as pigment in white paints. Another attractive feature has been the enhanced performance under real outdoor conditions or indoor applications (relatively better than competitors at diffuse light and higher temperatures). Other advantages for DSSCs also include flexibilities in the designs (transparency and multicolor options for building integration and consumer products etc.), lightweight, short energy payback time (<1 year), bifacial cells capturing light from all angles etc. Although the efficiencies of DSSCs at the present stage are lower than those conventional solar cells, the high ratio of the performance/price still identifies DSCs as an attractive potential solar cell technology to be commercialized.

2.3 Structure and Components of Dye Sensitized Solar Cell

The main parts of single junction dye sensitized solar cell are illustrated schematically in Figure 2.3. The cell is composed of four elements, namely, the transparent conducting and counter conducting electrodes, the nanostructure wide band gap semiconducting layer, the dye molecules (sensitizer), and the electrolyte. The transparent conducting electrode and counter-electrode are coated with a thin conductive and transparent film such as fluorine doped tin dioxide (F: SnO_2).

2.3.1 Transparent Substrate

Clear glass substrates are commonly used as substrate because of their relative low cost, availability and high optical transparency in the visible and near infrared regions of the Electromagnetic spectrum. Plastic and some metal plate are also used for flexible dye sensitized solar cells. Conductive coating (film) in the form of thin transparent conductive oxide (TCO) is deposited on one side of the substrate. The nanostructure wide band gap oxide semiconductor (electron acceptor) is applied, printed or grown on the conductive side. Before assembling the cell the counter electrode must be coated with a catalyzing layer such as graphite layer to facilitate electron donation mechanism to the electrolyte (electron donor).

The costs of producing a transparent conducting material depend on the cost of the raw materials and the processing of it into a thin layer. The cost of the raw materials generally increases in this order: Cd <Zn<Ti< Sn< Ag< In.

The costs of the deposition methods typically increase in the following order: Atmospheric pressure CVD<Vacuum Evaporation <Magnetron Sputtering<Low-Pressure CVD < Sol-gel <Pulsed Laser Deposition. The speed of the process is also very important in determining the cost.

The transparency levels of the transparent conducting electrode after being coated with the conductive film is not 100% over the entire visible and near

infrared (NIR) part of the solar spectrum. In fact, the deposition of nanostructure material reduces transparency of the electrode. Figure 2.4 shows a typical transmittance measurement (using dual beam spectrophotometer) of conductive glass electrode before and after being coated with nanostructure TiO_2 layer.

2.3.2 Nanostructure Photoelectrode

In the old generations of photoelectrochemeical solar cells (PSC) photoelectrodes were made from bulky semiconductor materials such as Si, GaAs or CdS. However, these kinds of photoelectrodes when exposed to light they undergo photo corrosion that results in poor stability of the photoelctrochemical cell. The use of sensitized wide band gap semiconductors such as TiO_2, ZnO_2 or SnO_2 resulted in high chemical stability of the cell due to their resistance to photo corrosion. The problem with bulky single or poly-crystalline wide band gap is the low light to current conversion efficiency mainly due to inadequate adsorption of sensitizer because of limited surface area of the electrode. One approach to enhance light-harvesting efficiency (LHE) and hence the light to current conversion efficiency is to increase surface area (the roughness factor) of the sensitized photoelectrode.

Due to the remarkable changes in mechanical, electrical, magnetic, optical and chemical properties of nanostructure materials compared to its phase in bulk structures, it received considerable attention. Moreover, because the area occupied by one dye molecule is much larger than its optical cross section for light capture, the absorption of light by a monolayer of dye is insubstantial. It has been confirmed that high photovoltaic efficiency cannot be achieved with the use of a flat layer of semiconductor or wide band gap semiconductor oxide surface but rather by use of nanostructure layer of very high roughness factor (surface area).The Doctor Blade method can be used to deposit nanoparticles suspension uniformly on a cleaned (rinsed with ethanol) substrate plate.

2.3.3 Fluorine Doped Tin Oxide (F:SnO$_2$) Semiconductor Crystal

Fluorine doped tin oxide film (FTO) is an n-type wide band gap semiconductor and has high transmittance in visible region, excellent conductivity, greater carrier mobility and good mechanical stability. An atomic displacement in the SnO$_2$ crystalline lattice in the neighborhood of the F-dopant is shown in Figure 2.5.

One of the O atoms situated in the central part of the super cell was replaced by an F atom. As a result, atoms in the neighborhood of the defective region have a tendency to displace themselves in order to find new equilibrium positions. The Sn

atoms move outwards the impurity doping by approximately 0.13 Å for Sn(1), and

0.16 Å for the Sn(2) and Sn(3), meanwhile the O atoms have a tendency to displace themselves towards the impurity by 0.04 Å in case of O(5), O(6), O(7) and O(8) atoms. The value of the displacement is not the same for all O atoms since O(10), O(11), O(12) and O(13) atoms shifts only by 0.01 Å. Finally, the O(9) atom does not experience any distortion from its original site. The pure and fluorine doped SnO$_2$ has tetragonal rutile structure. The Sn atoms move towards the impurity while the O atoms move outwards the defect. It is worth to mention that O(9) atom, which has not changed its initial distance with the defect, is the closest O atom to impurity, and has chemical bonds with Sn(3) and Sn(4) atoms. Thus, O(9) atom is trying to preserve its bond length with these tin atoms, and that explains why the distance between the impurity and the O(9) atom remains unchanged. The fact, that Coulomb electrostatic interaction is responsible for the atomic distortion. Density of States (DOS) pattern or Energy Band diagram for F-doped tin dioxide is shown in Figure 2.6. It is possible to observe that the Fermi level has been displaced from the top of the occupied states, and now it is situated at the bottom of the conduction band (CB), which means that the introduction of the fluorine impurity, which brings to the system one extra valence electron, produces a metallic state in the CB and

leads to the *n*-type electrical conductivity. That is in accordance to a number of available experimental observations.

2.3.4 Photosensitizer

Dye molecules of proper molecular structure are used to sensitized wide band gap nanostructure photo electrode. Upon absorption of photon, a dye molecule adsorbed to the surface of say nanostructure semiconductor (e.g.TiO_2, SnO_2) gets oxidized and the excited electron is injected into the nanostructure semiconductor. Among the first kind of promising sensitizers were Polypyridyl compounds of Ru(II) that have been investigated extensively. Many researchers have focused on molecular engineering of ruthenium compounds. For dye molecule to be excellent sensitizer, it must possess several carbonyl (C=O) or hydroxyl (-OH) groups capable of chelating to the metal sites on the semiconductor's surface. Figure 2.7 shows the molecular structure of some chemical dyes.

2.3.5 Redox Electrolyte

Liquid electrolytes typically consist of a redox couple and additives dissolved in a liquid solvent. The electrolyte undertakes the responsibility of dye regeneration and charge transport between the working electrodes (WEs) and counter electrodes (CEs).Electrolyte containing I^-/I_3^- redox ions is commonly used in DSSC to regenerate the oxidized dye molecules and hence completing the electric circuit by mediating electrons between the nanostructured electrode and counter electrode. NaI, LiI and R_4NI (tetra-alkyl ammonium iodide) are well known examples of mixture of iodide usually dissolved in nonprotonic solvents such as acetonitrile, propylene carbonate and propionitrile to make electrolyte. Cell performance is greatly affected by ion conductivity in the electrolyte which is directly affected by the viscosity of the solvent. Thus, solvent with lower viscosity is highly recommended. Moreover, counter cations of iodides such as Na^+, Li^+, and R_4N^+ do affect the cell performance mainly due to their adsorption on nanostructure electrode or ion conductivity. It has been

found that addition of tert-butylpyridine to the redoxing electrolyte improves cell performance. Br^-/Br_3^- redox couple was used in DSSCs and promising results were obtained. The V_{oc} and I_{sc} increased for the Eosin Y-based DSSC when the redox couple was changed.

The redoxing electrolyte needs to be chosen such that the reduction of I_3^- ions by injection of electrons is fast and efficient. This arise from the fact that the dependence of both hole transport and collection efficiency on the dye-cation reduction and I^-/I_3^- redox efficiency at counter electrodes are to be taken into account. In organic hole conductors, organic conducting polymers and organic hole conductors have also been tested in solid-state DSSCs (SDSSCs) to avoid the leakage and evaporation of liquid electrolytes. However, the poor pore infiltration of the mesoporous TiO_2 film with hole conductors in SDSSCs has so far remained a big challenge.

2.4 Operating Principle of Dye Sensitized Solar Cell

Nanocrystalline semiconductor is deposited on the conducting electrode (photo electrode) to provide the necessary large surface area to adsorb sensitizers (dye molecules). Upon absorption of photons, dye molecules are excited from the highest occupied molecular orbital (HOMO) to the lowest unoccupied molecular orbital (LUMO) states. Once an electron is injected into the conduction band of the wide band gap semiconductor nanostructure semiconductor film, the dye molecule (photo sensitizer) becomes oxidized (D^+). The injected electron is transported between the semiconductor nanoparticles and then extracted to a load where the work done is delivered as an electrical energy. Electrolytes containing I^-/I_3^- redox ions are used as an electron mediator between the semiconductor photo electrode and the carbon coated counter electrode. Therefore, the oxidized dye molecules (photo sensitizer) are regenerated by receiving electrons from the I^- ion redox mediator that get oxidized to I_3^- (Tri-iodide ions). The I_3^- substitutes the internally donated electron with that from the external load and reduced back to I^- ion. The

movement of electrons in the conduction band of the wide band gap nanostructure semiconductor is accompanied by the diffusion of charge-compensating cat ions in the electrolyte layer close to the nanoparticle surface. Therefore, generation of electric power in DSSC causes no permanent chemical change or transformation.

The maximum potential produced by the cell is determined by the energy separation between the electrolyte chemical potential (E_{redox}) and the Fermi level (E_F) of the semiconductor layer. The small energy separation between the HOMO and LUMO ensures absorption of low energy photons in the solar spectrum. Therefore, the photocurrent level is dependent on the HOMO-LUMO levels separation. This is analogous to inorganic semiconductors energy band gap (E_g). In fact, effective electron injection into the conduction band of semiconductor is improved with the increase of energy separation of LUMO and the bottom of the semiconductor conduction band. Furthermore, for the HOMO level to effectively accept the donated electrons from the redox mediator, the energy difference between the HOMO and redox chemical potential must be greater. Figure 2.8 shows a schematic representation of energy band structure of typical dye-Sensitized Solar Cells.

2.5 Photovoltaic Performance

Figure 2.9 shows the magnitude of the photocurrent and voltage curve to calculate cell efficiency.

Generation of electrical power under illumination is achieved by the capability of the photovoltaic device to produce voltage over an external load and current through the load at the same time. This is characterized by the current-voltage (IV) curve of the cell at certain illumination and temperature is shown in Figure 2.9. When the cell is short circuited under illumination, (the maximum current) the short circuit current (I_{SC}), is generated, while under open circuit conditions no current can flow and the voltage is at its maximum, called the open circuit voltage (V_{OC}). The point in the IV-curve yielding maximum product of current

and voltage, i.e. power, is called the maximum power point (MPP). Another important characteristic of the solar cell performance is the fill factor (FF), defined as

$$FF = \frac{I_{max}V_{max}}{I_{sc}V_{oc}} \qquad \ldots\ldots\ldots (2.1)$$

Using the fill factor, the maximum power output of the solar cell can be written as

$$P_{max} = V_{oc} \times I_{sc} \times FF \qquad \ldots\ldots\ldots (2.2)$$

While the physical principles behind the operation of different types of photovoltaic cells are generally different, the current-voltage curve of well performing cells are similar, and can be characterized and compared with each other in terms of FF, V_{OC}, and I_{SC}.

Finally, the energy conversion efficiency of the solar cell is defined as the power produced by the cell (P_{MAX}) divided by the power incident on the representative area of the cell (P_{light}):

$$\eta = \frac{V_{oc}I_{sc}FF}{P_{light}} \qquad \ldots\ldots\ldots (2.3)$$

The efficiency of the solar cell depends on the temperature of the cell, and which is even more important, on the quality of the illumination, i.e. the total light intensity and the spectral distribution of the intensity. For this reason, a standard measurement condition has been developed to facilitate comparable testing of the solar cells between different laboratories. In the standard condition used for testing of terrestrial solar cells the light intensity is 1000 W/m^2, the spectral distribution of the light source is that of AM1.5 global standard solar spectrum Figure 2.1 and temperature of the cell is 25°C. The power output of the solar cell at these conditions is the nominal power of the

cell, or module, and is reported in *peak* watts, W_p. In practice, special solar simulator light sources are used for the standard measurements.

2.6 The Incident Photon to Current Conversion Efficiency Measurement

The incident photon to current conversion efficiency (IPCE) measurement is another conventional measurement to quantitatively evaluate the spectral response of a DSC device. The IPCE value corresponds to the ratio of photocurrent density in the external circuit divided by the monochromatic photon flux, and can be calculated according to equation 2.4, where J_{ph} is the short-circuit current density generated by the monochromatic light, λ and P_{in} are the wavelength and light intensity, respectively. The IPCE describes how efficiently the incident photons are converted to electrons. The IPCE value can also be expressed as equation 2.5, where LHE is the light harvesting efficiency; Φ_{inj} and Φ_{reg} represent the quantum yields of electron injection and dye regeneration, respectively; and η_{cc} is the charge collection efficiency. J_{sc} in full sunlight can be calculated by the integral of the obtained IPCE spectrum. Note that a discrepancy of the J_{sc} between the value from the I-V measurement and the integrated one from the IPCE spectrum might exist since the IPCE is typically recorded at lower light intensities.

$$\text{IPCE} = 1240 \frac{J_{ph}}{\lambda P_{in}} \qquad \ldots\ldots\ldots (2.4)$$

$$\text{IPCE} = (\text{LHE}) (\Phi_{inj}) (\Phi_{reg}) (\eta_{cc}) \quad \ldots\ldots\ldots (2.5)$$

2.7 Characterization of the Samples

Material characterization is essential to understand the nature of things. It is requires that technique selection be matched to the form of the sample and

physical basis of the analytical probe. Characterization always follows a logical progression in which composition, crystallography, microstructure and physical properties are tested sequentially. In this experiment, the FTO films are characterized to determine their structural, electrical and opticl properties .The characterization techniques include X-ray diffraction (XRD), scanning electron microscopy (SEM) measurement, Sheet resistance measurement, VU-Vis response measurement, and Ellipsometery measurement.

2.7.1 X-ray Diffractometer (XRD)

X-ray Diffraction (XRD) is an important tool to determine long-range structural order. The diffraction patterns record the crystallography of the sample. This technique has been applied to many research areas to solve long range order structure of complex structures including proteins. X-ray diffraction (XRD) is a powerful technique .It is the most widely used for the identification of unknown crystalline materials (e g - minerals, inorganic compounds). Other applications are the characterization of crystalline materials, identification of fine - grained materials such as clays and mixed layer clays that are difficult to determine optically, determination of unit cell dimensions and measurement of sample purity. XRD is also used to determine the thickness of thin films and multilayer and atomic arrangements in amorphous materials (including polymers) and at interfaces.

In addition, the XRD technique can be used to obtain on formation on grain size, texture of grains, crystal defect densities, and thin film interdiffusion. There are three different types of XRD techniques, the Laue   method, the rotating crystal method, and the powder method, which carried out by either varying the Bragg's angle or the X-ray wavelength values. The photograph and the simplified diffraction system of the RIGAGU-RINT 2000 X-ray diffractometer is shown in Figure 2.10 and 2.11 respectively.

The Laue method: In this method, a stationary single crystal is bombarded with an X-ray beam of varying wavelength. The Laue method is capable of indicating the symmetry of crystal and can be used to determine the orientation of single crystal.

The rotating crystal method: The method utilizes a single crystal rotating in a beam of fixed wavelength X-ray. This technique is employed in this project for determining of crystal structure changes before and after heating cycle.

The powder method: This technique employs monochromatic radiation and finely powdered, or fine- grained polycrystalline specimen. In this case, a fixed beam's wavelength is used with a varying angle; this method can be used to determine lattice parameters accurately.

X-ray diffractometer consist of three basic elements: an X-Ray tube, a sample holder and X-ray detector. X-rays are generated in a cathode ray by heating a filament to produce electrons, accelerating the electrons towards a target by applying a voltage and bombarding the target material with electrons. When electrons have sufficient energy to dislodge inner shell electrons of the target material, characteristic X-rays spectra are produced. The spectra consist of several components, the most common being K_{α} and K_{β}. K_{α} consists of $K_{\alpha 1}$ and $K_{\alpha 2}$. $K_{\alpha 1}$ has a slightly shorter wavelength and twice the intensity as $K_{\alpha 2}$. The specific wavelengths are characteristic of the target material (Cu, Fe, Mg, Cr). Copper is the most common target material for single- crystal diffraction, with Cu K_{α} radiation. Filtering, by foils or crystal monochrometers, is required to produce monochromatic X-rays needed for diffraction. These X-rays are collimated and directed onto the sample. As the sample and detector are rotated, the intensity of the reflected X-ray is recorded.

X-ray diffraction patterns were performed using a RIGAGU-RINT 2000 X-ray diffractometer with Cu K alpha radiation of wavelength 1.54056 Å. The tube voltage is 40 KV and the tube current is 20 mA for the whole operation.

The crystallite size of the particle can be calculated from the XRD peak broadening of the (311) peak using the Scherrer's formula.

$$g_{crystallite} = \frac{0.9\lambda}{D\cos\theta} \qquad\qquad \text{........ (2.6)}$$

where, 'g' is the size of the crystallites, 'λ' is the wavelength of the X-ray used, '*D*' is the full width at half maximum height and '*θ*' is the angle of diffraction. The lattice parameter of the crystal can be derived using the following expression.

$$a = \frac{\lambda\sqrt{(h^2 + k^2 + l^2)}}{2\sin\theta} \qquad\qquad \text{......... (2.7)}$$

where, 'a' is lattice parameter (Å), 'λ' is the wave length of the radiation (Å), 'θ' is the Bragg's angle and (hkl) are Miller indices. In this research, we used Cu Kα radiation in which λ = 1.54056 Å.

The theoretical density is X-ray density ρ_x of the sample can be calculated according to the relation given by Smith and Wijin,

$$\rho_x = \frac{8M}{N_a a^3} \qquad\qquad \text{........... (2. 8)}$$

where, 'M' is molecular mass of the sample, '8' is the number of molecules in the unit cell, 'N_a' is the Avogadro's number and 'a' is the lattice parameters.

2.7.2 Scanning Electron Microscopy (SEM)

The scanning electron microscopy (SEM) is now widely used not only in medical science and biology but in diverse fields such as materials development, metallic materials, ceramics and the semiconductor industries. The electron microscope has become a very important part of materials structure determination. Scanning electron microscopy (SEM) was the electron reflected to form the image, such that the thickness of the sample is not important. SEM can be used to image over a very large magnification range

from 1 μm to 100 μm, allowing study of particle morphology band size, surface texture and detail defects in surface such as faults and cavities cause by etching or corrosion. SEM creates images of the surface with depth perception, which is much better than optical microscopy and at a magnification that can be a few orders of magnitude higher. The most common use of SEMs for superconductor applications is to view the grain size of chemical compositions, bond structure analysis and cross-section analysis to determine device dimension. The scanning electron microscope (SEM) is the most widely used type of electron microscope. It examines microscopic structure by scanning the surface of materials, similar to scanning co focal microscopes but with much higher resolution and much greater depth of field. It is used to study surface morphology. Scanning Electron Microscopy (SEM) is a technique whereby a beam of energetically well-defined and highly focused electrons is scanned across a material (sample). The microscope uses a lanthanum hex boride source and is pumped using turbo and ion pumps to maintain the highest possible vacuum. The technique can provide material's (only conducting and semi conducting) information about topography, morphology and crystallography.

The basic principle of the system is that, the electron beam impinges the surface and generates a splash of electrons with kinetic energies much lower than the primary incident electrons called secondary electrons. An image of the sample surface is constructed by measuring the secondary electron intensity as a function of the primary beam position. The SEM also has much higher resolution, so closely spaced specimens can be magnified at much higher levels. Because the SEM uses electromagnetic lenses, the researcher has much more control in the degree of magnification. All of these advantages, as well as the actual strikingly clear images, make the scanning electron microscope one of the most useful instruments in research today. The SEM provides a highly magnified image of the surface of a material that is very similar to what one would expect if one could actually "see" the surface visually .The resolution of the SEM can approach a few nano meter and it can operate at magnification

that are easily adjusted from about 10X- 300,000X. The micrographs of thin films were obtained using JEOL Scanning Electron Microscope model JSM – 5610 LV. The photograph and the simplified layout of SEM are shown in Figure 2.12 and Figure 2.13 respectively.

2.7.3 Spectroscopic Ellipsometry

Ellipsometry is a very sensitive measurement technique that uses polarized light to characterize thin films, surfaces, and material microstructure. The main advantages of ellipsometry are its non-destructive character, its high sensitivity related to the measurement of the phase of the reflected light, its wide measurement range (from fractions of single layers to micrometers), and the possibility to control in real time complex processes. On the contrary, the main bottlenecks are the very complex analysis and the costs of ellipsometric setups which are commonly rather high.

If a linearly polarized light of a known orientation is reflected at oblique incidence by a surface, the reflected light is elliptically polarized . The shape and orientation of the ellipse depend on the angle of incidence, the direction of polarization of the incident light, and the reflection properties of the surface. Ellipsometry measures two values, Psi (Ψ) and Delta (Δ), that describe this polarization change. These values are related to the ratio of Fresnel reflection coefficients, $\tilde{R}_p$ and $\tilde{R}_s$ for p- and s-polarized light, respectively by the following equation:

$$\rho \equiv \frac{\tilde{R}_p}{\tilde{R}_s} = \tan(\psi) \cdot e^{i\Delta} \qquad \ldots\ldots\ldots (2.9)$$

Since ellipsometry measures the ratio of two values, it can be highly accurate and very reproducible. In general the ratio is a complex number, thus it contains "phase" information (Δ) which makes the measurement very sensitive. The

phase information increases the sensitivity to the surface condition to a great extent, allowing the study of ultra-thin films even at a sub-monolayer level.

All ellipsometer setups are composed by a light source and a detector. The arrangement of the optical components between the source and detector defines the type of the specific ellipsometer. Ellipsometers utilize two polarizers, one placed before the sample and the other (often called analyzer) placed just prior to the detector. Some ellipsometer arrangements use also a modulator (or compensator) placed between polarizer and sample. In particular, spectroscopic measurements provide many information about the sample and also provide the ability to acquire data in spectral regions where the measured data are most sensitive to the model parameters which are to be determined.

In spite of it's extremely sensitivity, ellipsometry has not been widely used in the past because it is an indirect measurement requiring the computational power of modern computers. Ellipsometry does not measure directly the optical constants or film thickness, but Ψ and Δ, which, however, are functions of these characteristics. Film thickness and all optical constants must be extracted through a careful and rather sophisticated analysis based on different models. After measurement, the first step in data analysis is to build a model of the material. This model needs to include the order of the layers, their optical constants and their thickness. If these values are not known, a "best guess" should be entered. Next, data must be generated from the model and then compared to the experimental data. If the starting values of the unknown parameters are too far off, the regression algorithm will get lost and we have to restart from the "model" step changing fit parameter values or building a new model. Standard softwares for data analysis are based on the mean squared error (MSE) to quantify the difference between experimental and calculated model data: a smaller MSE implies a better fit.

Levenberg-Marquardt algorithms are commonly used to quickly minimize the MSE value. In our laboratory a spectroscopic ellipsometer VASE® produced by J.A. Woollam Co is available; the VASE® is a Variable Angle Spectroscopic

Ellipsometer which exploits the rotating analyzer configuration. The setup is equipped with a computer-controlled retarder (AutoRetarderTM) which allows measurement of Δ in the whole range 0-360° without ambiguity; the measurable spectral range is 190-1700 nm. The photograph and the simplified diagram of an ellipsometer are shown in Figure 2.14 and 2.15 respectively.

2.7.4 Ultraviolet and Visible (UV-Vis) Spectrophotometry

Spectrophotometer is an instrument that measures the fraction of the incident light transmitted through a solution. In other words, it is used to measure the amount of light that passes through a sample material and, by comparison to the initial intensity of light reaching the sample, they indirectly measure the amount of light absorbed by that sample. The photograph and the block diagram of the UV-VIS-1800 spectrophotometer are shown in Figure 2.16 and 2.17 respectively.

A given compound will not absorb all wavelengths equally–that's why things are different colors (some compounds absorb only wavelengths outside of the visible light spectrum). Because different compounds absorb light at different wavelengths, a spectrophotometer can be used to distinguish compounds by analyzing the pattern of wavelengths absorbed by a given sample. Additionally, the amount of light absorbed is directly proportional to the concentration of absorbing compounds in that sample, so a spectrophotometer can also be used to determine concentrations of compounds in solution. Finally, particles in suspension will scatter light (thus preventing it from reaching the light detector), spectrophotometers may also be used to estimate the number of cells in suspension.

Visible light (400 nm - 700 nm) constitutes only a small portion of the spectrum that ranges from gamma rays (less than 1 pm long) to radio waves that are thousands of meters long. When studying a sample by spectrophotometry, we put it in a sample holder called a cuvetteand place it in the spectrophotometer. Light of a particular wavelength passes through the sample inside the cuvette and the amount of light transmitted (passed through the solution— Transmittance) or absorbed (Absorbance) by the sample is measured by a light meter.

A spectrophotometer can display measurements as either transmittance or absorbance. The amount of light transmitted through a sample is referred to as transmittance (T).

Absorbance (A) is related logarithmically to transmission thusly.

$$A = - \log T \quad \ldots\ldots\ldots (2.10)$$

The light from the spectrophotometer's light source (in the case of measurements in the visible range, a simple incandescent bulb) does not consist of a single wavelength, but a continuous portion of the electromagnetic spectrum. This light is separated into specific portions of the spectrum through the use of prisms or a diffraction grating. A small portion of the separated spectrum then passes through a narrow slit.

When you adjust the wavelength on a spectrophotometer, we are changing the position of the prism or diffraction grating so that different wavelengths of light are directed at the slit. The smaller the slit width, the better the ability of the instrument to resolve various compounds. The slit width is < 8 nm. Very high quality spectrophotometers have slit widths of < 2 nm. This small band of light then passes through the curette containing the sample. Light that passes through the sample is detected by a photocell and measured to yield the transmittance or absorbance value (optical density) for the sample.

Transmittance values can be easily derived from the formulas given above. In equation form,

$$T = \frac{I}{I_o}$$ .... (2.11)

where I_0 is the intensity of the incident light and I is the intensity of the light coming out of the sample. In these equations, scattering and reflection are considered to be close to zero or otherwise accounted for. The transmittance of a sample is sometimes given as a percentage. Transmittance is related to absorbance A (not to be confused with absorptance) as

$$A = -\log_{10} T = -\log 10 \left(\frac{I}{I_o} \right)$$ .... (2.12)

or using the natural logarithm

$$A = -\ln T = -\ln \left(\frac{I}{I_o} \right)$$ .... (2.13)

The optical absorption coefficient α is determined using the relation

$$\alpha = \left(\frac{2.303}{d} \right) \left[\log \left(\frac{1}{T} \right) \right]$$ .... (2.14)

where d is the thickness of the sample. In SI units, absorption coefficient is measured in inverse meters, and is represented by the Greek letter. In chemistry and biological sciences, the absorption coefficient is a measure of the solubility of a gas in a liquid measured as the volume of the gas (taken under standard conditions) that saturates a unit volume of the liquid.

2.8 Resistivity and Conductivity Measurement

Many resistors and conductors have a uniform cross section with a uniform flow of electric current and are made of one material.(as shown in Figure 2.18) the electrical resistivity ρ (Greek: rho) is defined as:

$$\rho = \frac{RA}{\ell}$$

……… (2.15)

where,

R is the electrical resistance of a uniform specimen of the material (measured in ohms, Ω)

ℓ is the length of the piece of material (measured in metres, m)

A is the cross-sectional area of the specimen (measured in square metres, m²).

The reason resistivity is defined this way is that it makes resistivity a material property, unlike resistance. All copper wires, irrespective of their shape and size, have approximately the same resistivity, but a long, thin copper wire has a much larger resistance than a thick, short copper wire. Every material has its own characteristic resistivity – for example, rubber's resistivity is far larger than copper's resistivity.

In a hydraulic analogy, passing current through a high-resistivity material is like pushing water through a pipe full of sand, while passing current through a low-resistivity material is like pushing water through an empty pipe. If the pipes are the same size and shape, the pipe full of sand has higher resistance to flow. But resistance is not solely determined by the presence or absence of sand; it also

depends on how wide the pipe is (it is harder to push water through a skinny pipe than a wide one) and how long it is (it is harder to push water through a long pipe than a short one.)

The above equation can be transposed to get Pouillet's law:

$$R = \rho\, l/A$$

………. (2.16)

The resistance of a given material will increase with the length, but decrease with increasing cross-sectional area. From the above equations, resistivity has SI units of ohm metre. Other units like ohm cm or ohm inch are also sometimes used.

The formula $R = \rho l/A$ can be used to intuitively understand the meaning of a resistivity value. For example, if $A = 1$ m^2 and $l = 1$ m (forming a cube with perfectly-conductive contacts on opposite faces), then the resistance of this element in ohms is numerically equal to the resistivity of the material it is made of in ohm-meters. Likewise, a 1 ohm cm material would have a resistance of 1 ohm if contacted on opposite faces of a (1 cm $\times$ 1 cm $\times$ 1 cm) cube.

Conductivity σ (Greek: sigma) is defined as the inverse of resistivity:

$$\sigma = 1/\rho$$

………. (2.17)

Conductivity has SI units of Siemens per metre (S/m)

2.9 Band Gap Energy Calculation

The nature of the transition (direct or indirect) involved during the optical absorption process can be determined by studying the dependence of absorption coefficient 'α' on photon energy 'hν'

$$\alpha(h\nu) = A(h\nu - E_g)^{n/2}$$

……… (2.18)

Where A is a constant, the value of n depends on the type of transition (direct: n = 1, direct forbidden: n = 3, indirect: n = 4, indirect forbidden n =6). If transitions occur between valance band wave functions derived from s-states of the individual atoms, and the conduction band from p-states, etc, the change in orbital quantum numbers is ± 1, and the transitions are allowed, irrespective of whether they are phonon assisted (indirect gap) or not (direct gap).

If the later were derived, for example, from d-states, thus involving orbital quantum number changes distinct from ± 1, the transitions are not allowed (are forbidden) as per conventional spectroscopic selection rules.

To determine whether the films have direct or indirect band gap, plots of $(\alpha h\nu)^2$ vs. (hν) and $(\alpha h\nu)^{1/2}$ vs. (hν) were plotted, where α is the optical absorption coefficient and hν is the photon energy. Better linearity was observed in the former case and it was determined that all the films have a direct band transition. The optical band gap values were obtained from optical absorption spectra by plotting $(\alpha h\nu)^2$ vs. (hν) then extrapolating the straight line portion to energy axis.
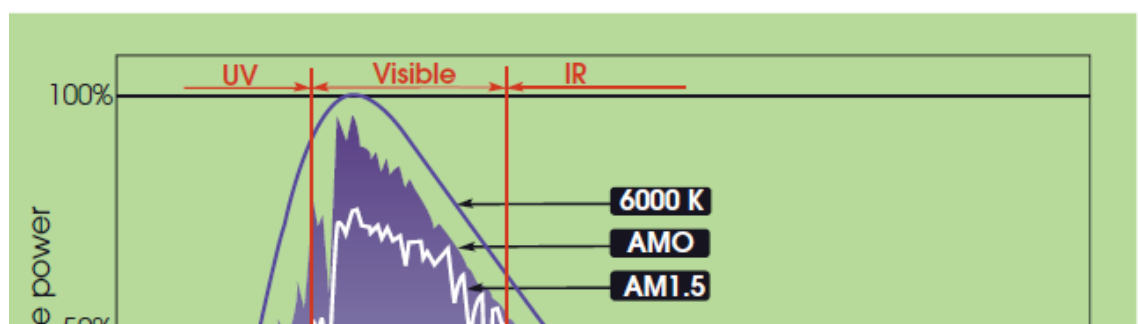
Figure 2.1The standard AM1.5 global solar spectrum.
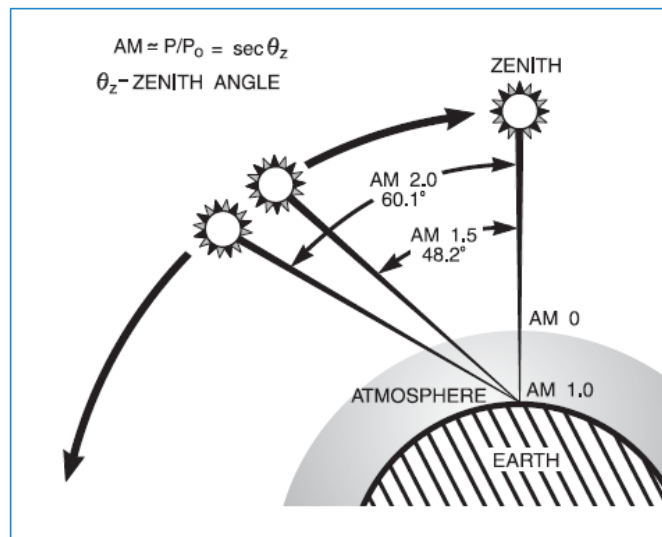
Figure 2.2 The path length in units of Air Mass, change with the zenith angle.
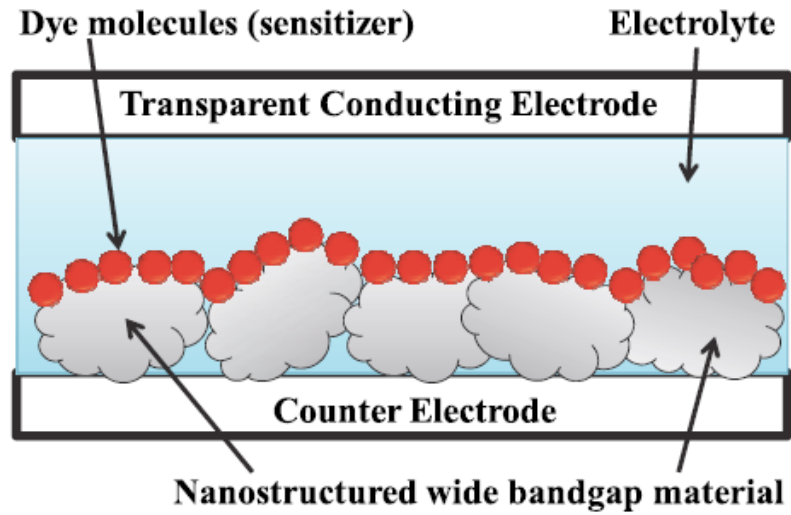
Figure 2.3 A schematic representation of the structure and components of the dye-

      sensitized solar cell.
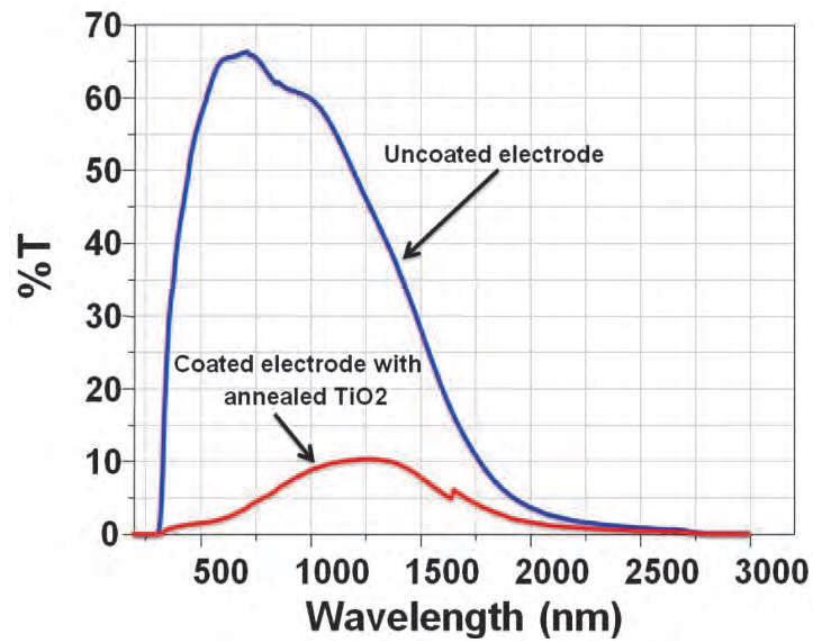
Figure 2.4 Transmittance of conductive glass electrode before and after being coated with nanostructure TiO_2 layer.
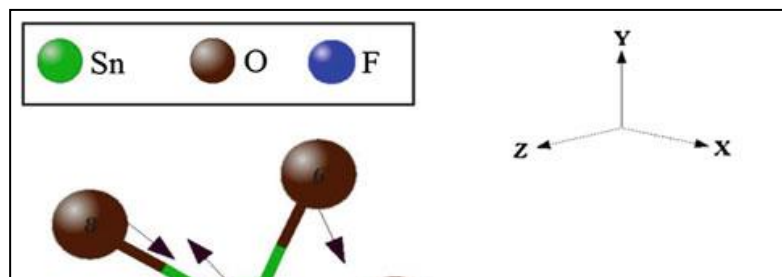
Figure 2.5 Atomic displacements in the SnO_2 crystalline lattice in the
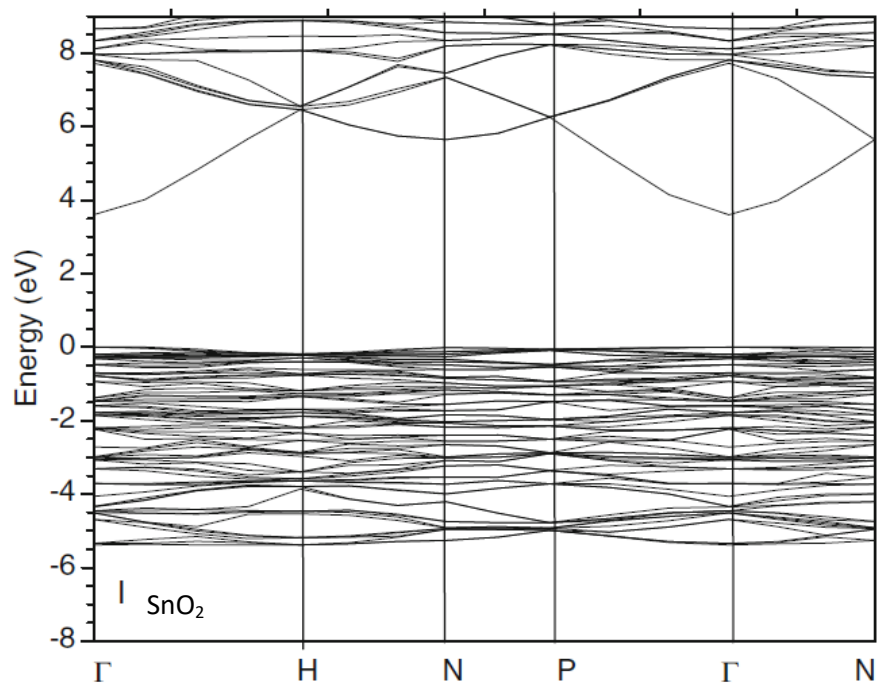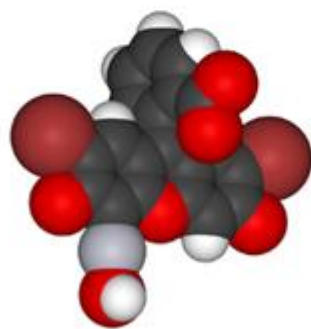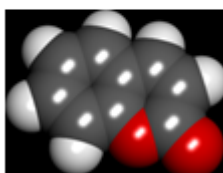neighborhood of the F-dopant

Figure 2.6 Band Structure of SnO_2.

$C_{20}H_8Br_2HgNa_2O_6$

$C_{16}H_{18}N_3SCl$

(a)

(b)

$C_9H_6O_2$
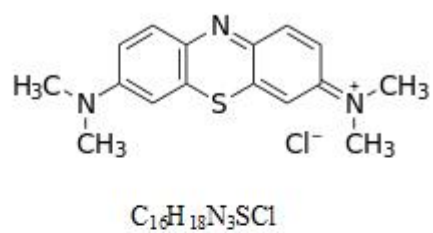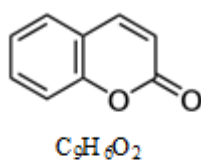
(c)

Figure 2.7 The molecular structure of some chemical dyes (a) Mercurochrome (b) Methyl blue dye (c) Coumarin dye.
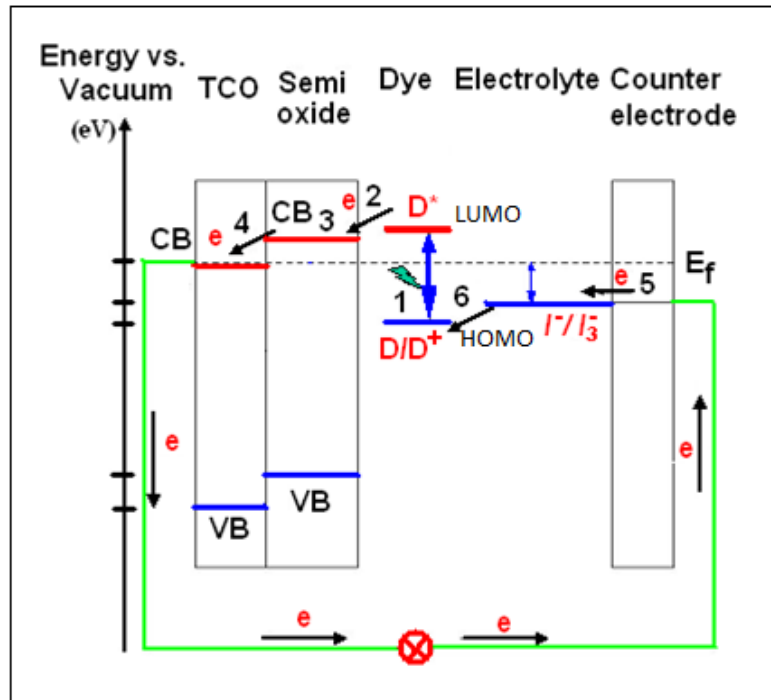
Figure 2.8 A schematic representation of energy band structure of a typical Dye-
sensitized Solar Cell.
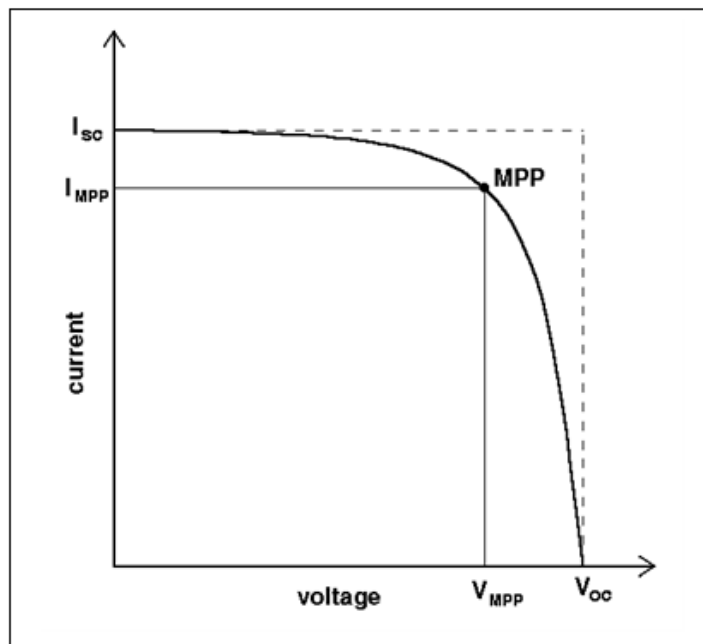
Figure 2.9 Typical shape of the current-voltage curve of a photovoltaic cell
showing the Open circuit voltage V_{OC}, short circuit current I_{SC}, and
the maximum power point MPP, and the current and voltage at the
MPP: IMPP, VMPP.

Figure 2.10 The RIGAGU–MultiFlex 2kW X–ray diffractometer
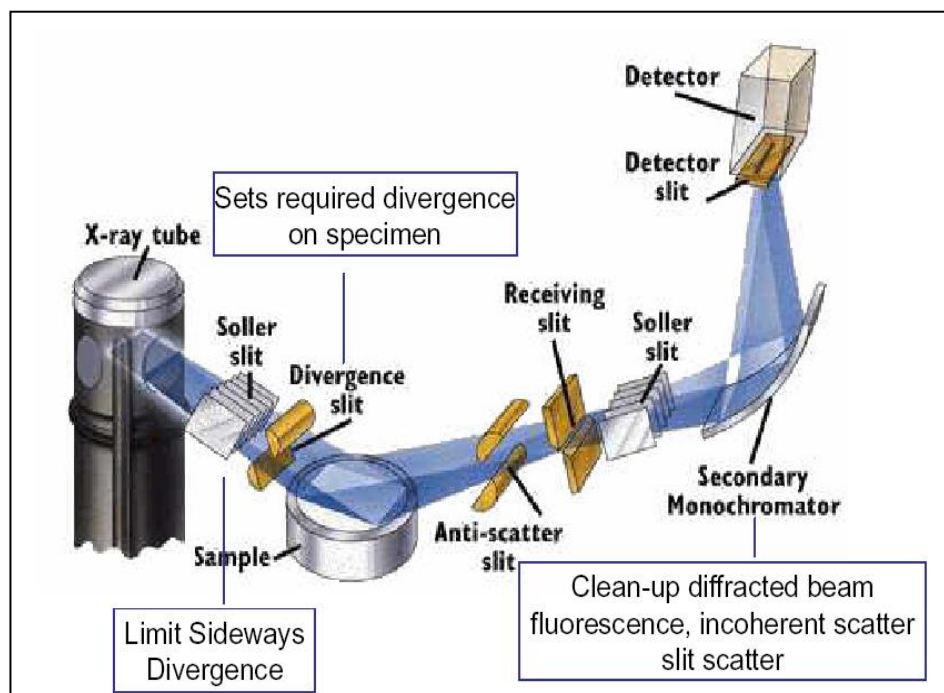
Figure 2.11 X-ray diffraction system configurations

Figure 2.12 The photograph of Scanning Electron Microscope (JEOL)
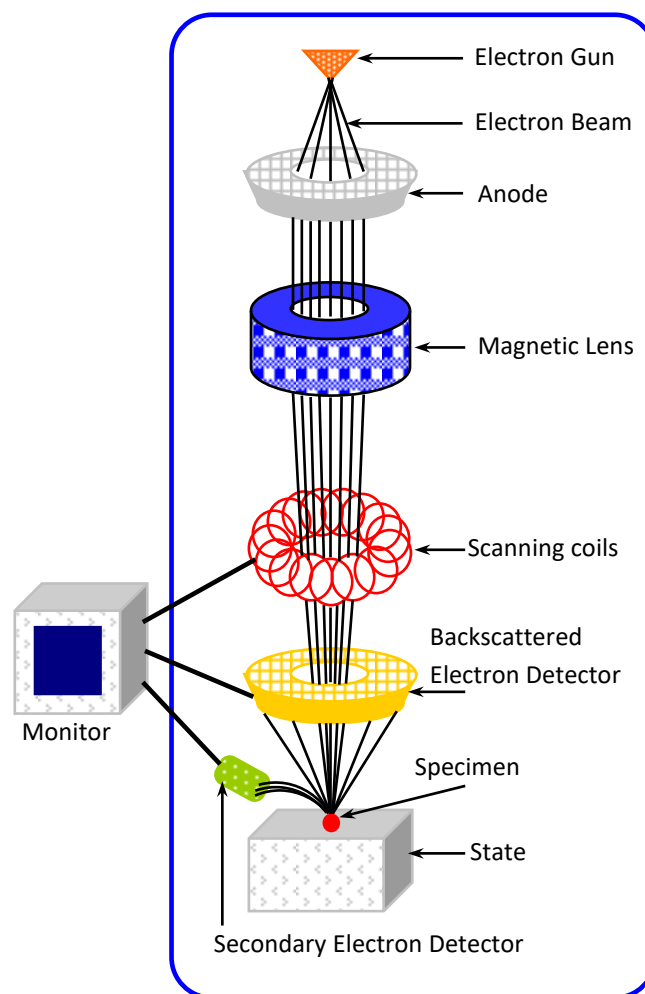
Figure 2.13 A simplified layout of a SEM

Fig 2.14 The photograph of two-angle Ellipsometer.
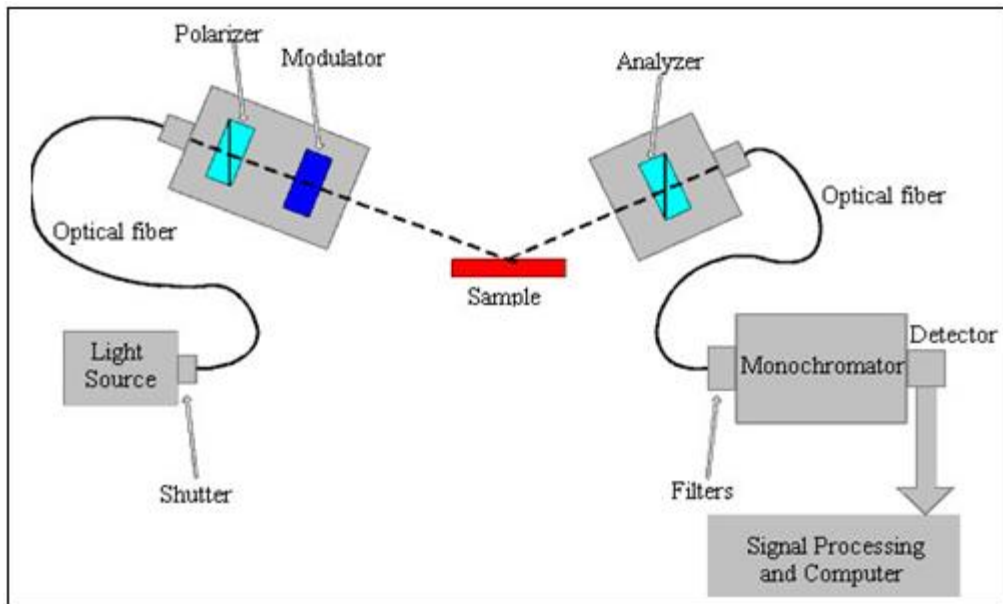
Figure 2.15 Diagram of an optical ellipsometer

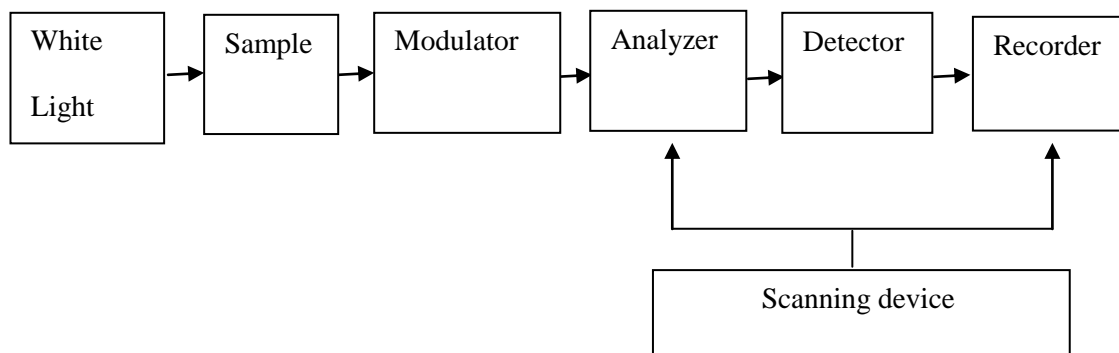Figure 2.16 Photograph of double beam spectrophotometer

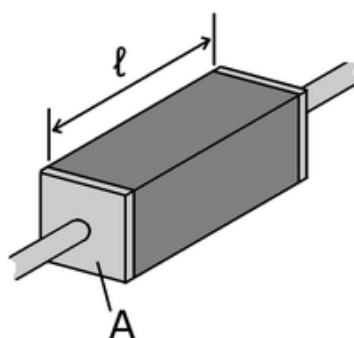Figure 2.17 Block diagram of an absorption spectrophotometer

Figure 2.18 A piece of resistive material with electrical contacts on both ends.

CHAPTER III

EXPERIMENTAL DETAILS

3.1 Preparation of Fluorine Doped Tin Oxide (F:SnO$_2$) Powder

Fluorine doped SnO$_2$ powder has been prepared by following sol-gel auto-combustion method. Firstly, 5.2g of SnCl$_4$.5H$_2$O, 0.4g of acetylene black and 0.38g of HF (50%) were weighed by digital balance. Then SnCl$_4$ and HF were dissolved in 20ml of deionized water. Acetylene black was added to this solution. NH$_4$OH aqueous solution was added drop wise during constant stirring as shown in Figure 3.2.After 15 min stirring, the solution turned to gel. This gel was heated at 120 °C for 10min to get dry gel. The dry gel was further heated at 500 C° in air. After 30min ignition of the dry gel, auto-combustion process took place as shown in Figure 3.3 and F doped SnO$_2$ powder was obtained. The colour of as-burnt powder is gray.

The sample was further calcined at 550 °C for 30min. The colour of the sample is light gray. The sample was sintered at 650 °C for 2 hours. The colour of the simple changed to yellow. The sample was sintered at 750 °C for 2 hours. The colour of the simple changed to white.

Finally, the nanoporous F doped SnO$_2$ powder has been successfully obtained. The structure and morphology was investigated by XRD and scanning electron microscopy (SEM).The crystallite size of the particle can be calculated from the XRD peak broadening of the (110) peak using the Scherrer's formula (equation 2.6).The lattice parameter of the crystal can be derived using the following expression.

$$\frac{1}{d^2} = \frac{h^2 + k^2}{a^2} + \frac{l^2}{c^2} \qquad \text{---------- (3.1)}$$

where, a and c are lattice parameters (Å), (hkl) are Miller indices and d is spacing between (h k l) planes.
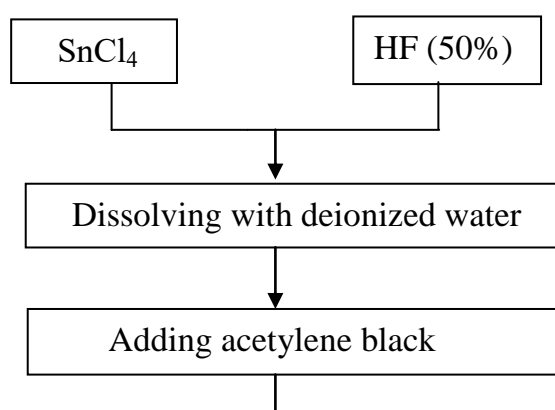
$$\boxed{\text{SnCl}_4} \qquad \boxed{\text{HF (50\%)}}$$

$$\boxed{\text{Dissolving with deionized water}}$$

$$\boxed{\text{Adding acetylene black}}$$

Figure 3.1. Flow chart of F:SnO$_2$ powder preparation .

3.2 F doped SnO$_2$ (FTO) Coating on Glass Substrates

3.2.1 Preparing the Precursor Solution

The solution was prepared by dissolving 13g (0.037mole) of tin chloride (SnCl$_4$.5H$_2$O) in 100 ml of ethanol. 0.84226g (0.02275mole) of ammonium fluoride (NH$_4$F) was then added into the solution for fluorine doping. 5ml of concentrated hydrochloric acid (HCl) was then added into the solution for

simultaneous condensation and gelation. The mixed solutions were well stirred and refluxed for one hour at 60° C. The solutions were filtered and cooled in the ambient as shown Figure 3.4. This solution could be used this day for spray pyrolysis coating method. Then the solution was aged in open beakers at room temperature for gelation to be used in spin coating method. In this research work sol-gel spin coating method and spray pyrolysis method have been used to prepare FTO films.

3.2.2 Cleaning the Glass Substrates

Firstly, glass substrates were sinked in the dilute HCl for 1 hour. Secondly, the glasses were treated with deionized water for 15mins. Thirdly, these glasses were treated with ethanol for 15mins.Fourthly, these glasses were boiled in the potassium dichromate solution. Finally, these glasses were washed with distilled water again and again and then the cleaned glass substrates were obtained by drying.

3.2.3 Coating the Glass Substrates by Spin Coating Technique

3ml of prepared gel was dispensed on the cleaned glass substrate mounted on the turn table spinning at 3000 rpm for 10 sec. After each spin coating, the samples were dried at 100°C for about 10 min. After 10 times of coating, the films were post heated at 325°C, 350°C, 375°C, 400°C, 425°C and 450°C respectively. Figure 3.5 and 3.6 show the photograph and schematic diagram of spin coating mechanism.

3.2.4 Coating the Glass Substrates by Spray Syrolysis Technique

The prepared solution was poured into a container of a spray gun which was set up at the top of the chamber vertically aligned with the substrate holder. The purified air at a pressure of 2 bars was used as a carrier gas and the flow rate from the spray nozzle was maintained perpendicular to the glass substrate. The distance between the glass substrate and spray nozzle was 300mm. The glass substrate temperature was 600°C which was controlled with the temperature

controller. One cycle of spray consists of a 5s spray time with and interval of 1.0s was repeated 400 spray times. As the temperature of the substrate was maintained constant, a FTO thin film exhibiting excellent homogeneity was formed on the substrate. Figure 3.7 and 3.8 show the photograph and schematic diagram of spin coating mechanism.

The structural, optical and electrical properties of the prepared films have been investigated by XRD, SEM , UV-Vis Spectrometer and Ellipsometer.

3.3 Fabrication Process of TCO-less Dye Sensitized Solar Cells

In this research DSSCs have been fabricated by the following steps.

3.3.1 Preparing the Working Electrodes

The well cleaned ordinary glasses have been used as substrates for preparing working electrodes. The scotch tape has been used to cover the three sides of the glass substrates. The nanoporous semiconductor paste was prepared by grinding 2.5 ml of citric acid (pH 2.4) and 1.5g of fluorine doped tin oxide powder in the mortar and pestle for about 30 minutes to break the aggregation of F: SnO2 powder. One drop of washing powder solution was added to this suspension to reduce surface tension. The resultant paste was put on the masked glass substrates. The flattened paste was distibuted by doctor's blade method. These electrodes were put on the hot plate and heated them at approximately 150℃ for 30 min and then cooled down slowly.

3.3.2 Preparing Dye Solutions

About 0.2 g of coumarin powder, mercurochrome and methyl blue were dissolved in 100 ml of ethanol in each beaker separately for about 3 hours. Coumarin dye solution is colourless, the mercuochrome solution has red colour and methyl blue solution has blue colour. The utraviolet-visible (UV-Vis) responses of the prepred dye solutions were investigated by UV-1800 Shimadzu spectrophotometer. From UV-Vis spectrum, the band gap of these dye solution have been estimated.

3.3.3 Dipping Working Electrodes in Dye Solutions

The prepared working electrodes were dipped in each dye solution for about (10-30) minutes depending on selected dye solutions and then dried in the dryer. These electrodes were heated mildly at (60-80℃) if coloration is too slow.

3.3.4 Preparing the Counter Electrodes

The cleaned ordinary glasses, silver coated glasses and FTO glasses (which were made in URC lab) were uses as substrates for preparing counter electrodes. The scotch tape was used to cover the three sides of the counter electrodes. The carbon enrich SnO_2 paste was prepared by grinding 2 g of SnO_2 powder, 0.4g of actylene black powder and 0.1 g of graphide powder with 10ml of ethanol and 0.1ml of Triton X-100 in mortar and pestle for about 1 hours. The prepared paste was put and flattened on each glass substrate by doctor's blade method. The counter electrodes were dried on the open hot plate (at about 150℃) and then cooled down slowly.

3.3.5. Preparing the Electrolyte Solution

The redox electrolyte solution was prepared by mixing 0.5M potassium iodide and 0.05M iodine in unhydrous ethylene glycol. This electrolyte was stored in dark coloured bottle for further use.

3.3.6 Filling Electrolyte Solution in the Holes and Binding two Electrodes

The spacer made by cutting plastic film is put on the cooled counter electrodes. Some of the electrolyte solution was dropped into the holes and the two electrodes were combined quickly to prevent the solvent from drying out. By fixing them with binder clips the experimental procedure for fabrication of TCO-less and with only TCO glasses involved DSSCs were completed.

Figure (3.9) shows the fabrication processes of DSSCs. Figure (3.10) shows the prepared working electrodes, counter electrodes and spacers. Figure (3.14) shows the schematic representation of the structure and components of the DSSC.
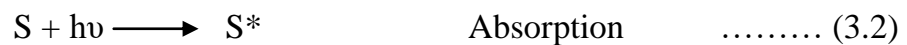
3.3.7 Measuring the Parameters of DSSCs

The open circuit voltage and short circuit current of constructed cells were measured by digital multimeter. To measure open circuit voltage (V_{OC}) and the short circuit current (I_{SC}) for each cell, the cell was connected with external circuits shown in Figure 3.11.

Figures 3.12 and 3.13 show the photographs for measuring currents and voltages under illuminations. The open circuit voltage V_{OC} and the short circuit current I_{SC} for each cell were measured under illumination of (1000 W/m^2) neon bulb and the effective cells' area is 1cm^2.

3.3.8 Working Principle of TCO-less DSSCs

Figure 3.14 shows the schematic representation of the structure and components of the dye-sensitized solar cells. Figure 3.15 shows the working principles of DSSCs. It can be demonstrated as the following equations.

At Cathode:

$$S + h\upsilon \longrightarrow S^* \qquad \text{Absorption} \qquad \text{......... (3.2)}$$

$$S^* \longrightarrow S^+ + \bar{e} \ (F:SnO_2) \ \text{Electron injection} \quad \text{......... (3.3)}$$

$$2S^+ + 3I^- \longrightarrow 2S + I_3^- \qquad \text{Regeneration} \qquad \text{.........(3.4)}$$

At Anode:

$$I_3^- + 2\bar{e} \ (\text{carbon}) \longrightarrow 3I^- \qquad\qquad\qquad \text{......... (3.5)}$$

Cell:

$$\bar{e}\,(\text{carbon}) + h\upsilon \longrightarrow \bar{e}\,(\text{F:SnO}_2) \qquad\qquad \dots\dots\dots\,(3.6)$$

Due to the energy level positioning in the system (Figure 3.14), the cell is capable of producing voltage between its electrodes and across the external load. The maximum theoretical value for the photovoltage at open circuit condition is determined by the potential difference between the conduction band edge of the SnO_2 and the redox potential of the I^-/I_3^- pair in the electrolyte. The operation of the cell is regenerative in nature, since no chemical substances are neither consumed nor produced during the working cycle, as visualized in the cell reaction. At its simplest configuration (Figure 3.14), the DSSC or the dye cell is comprised of a transparent glass electrode coated with porous nanocrystalline fluorine doped tin oxide (nc- $F:SnO_2$), dye molecules attached to the surface of the nc- $F:SnO_2$, an electrolyte containing a reduction-oxidation couple such as I^-/I_3^- and a catalyst coated counter-electrode. During illumination the cell produces voltage over and current through an external load connected to the electrodes.

Essential to the optical operation of this porous electrode structure is the fact that, nc- F:SnO2 as a large band gap semiconductor, absorbs light only below about 400 nm, letting the major part of the solar spectrum available for the dye molecules.

The absorption of light in the DSSC occurs by dye molecules and the charge separation by electron injection from the dye to the $F: SnO_2$ at the semiconductor electrolyte interface. A single layer of dye molecules however, can absorb only less than one percent of the incoming light. While stacking dye molecules simply on top of each other to obtain a thick dye layer increases the optical thickness of the layer, only the dye molecules in direct contact to the semiconductor electrode surface can separate charges and contribute to the

current generation. A solution to this problem was to use a porous nanocrystalline F:SnO$_2$ electrode structure in order to increase the internal surface area of the electrode to allow large enough amount of dye to be contacted at the same time by the F:SnO$_2$ electrode and the electrolyte (Figure 3.15).Having this construction, a F:SnO$_2$ electrode typically 10 μm thick, with an average particle (as well as pore) size typically in the order of 20 nm, has an internal surface area thousands of times greater than the geometrical (flat plate) area of the electrode.
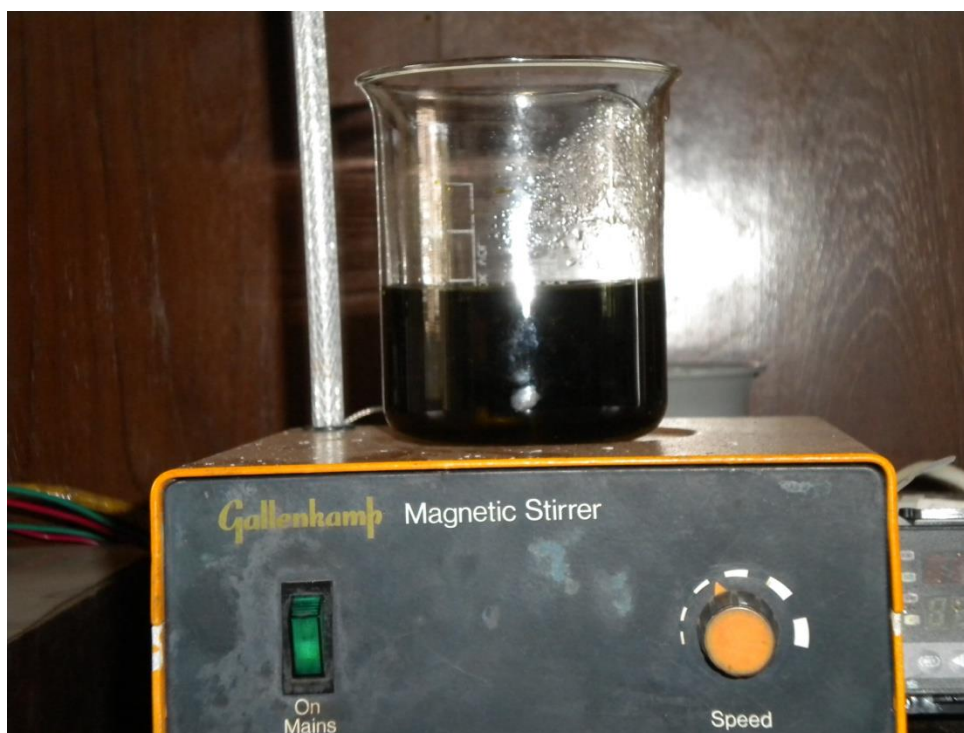
Figure 3.2. The photograph of constant stirring solution

Figure 3.3. The photograph of auto-combustion process (at 500°C).

Figure 3.4 The filtered precursor solution for FTO coating.

Figure 3.5 The mechanism of the spin coater.

Spin coating

Drying(100°C)

Pre-sintering(200°C

Stacking
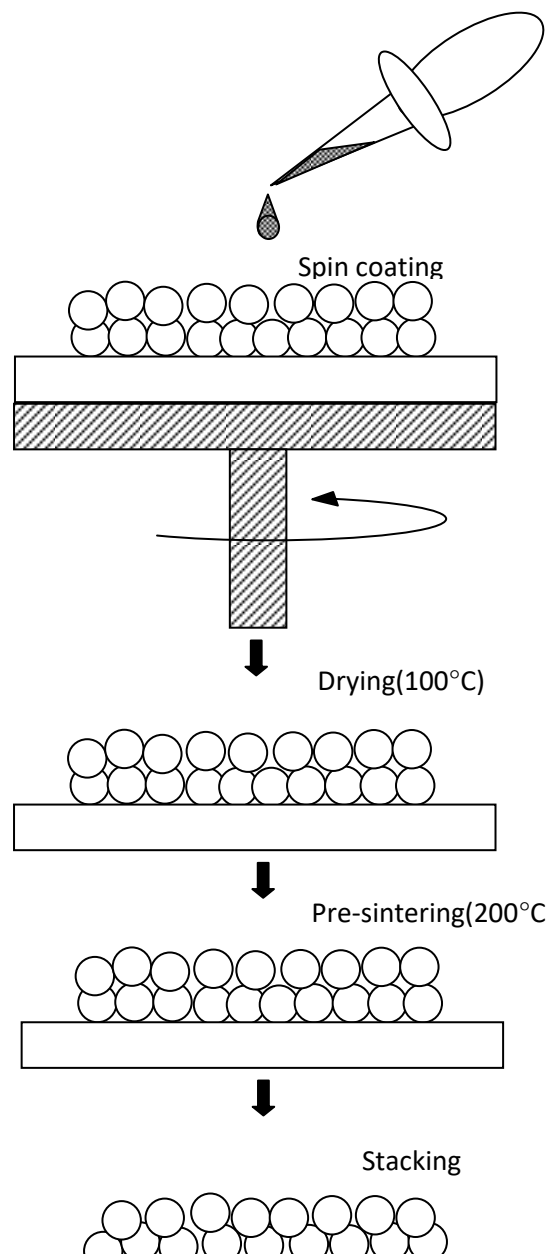
Figure 3.6 The schematic diagram of formation of F:SnO$_2$ electrode by the spin coating technique.
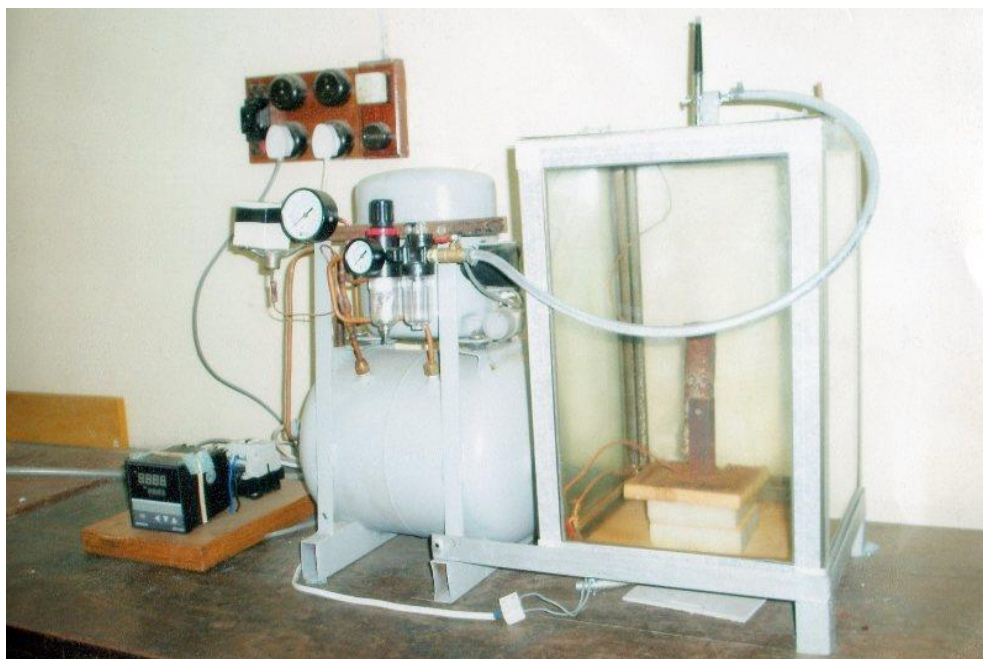
Figure 3.7 Complete Spray pyrolysis system
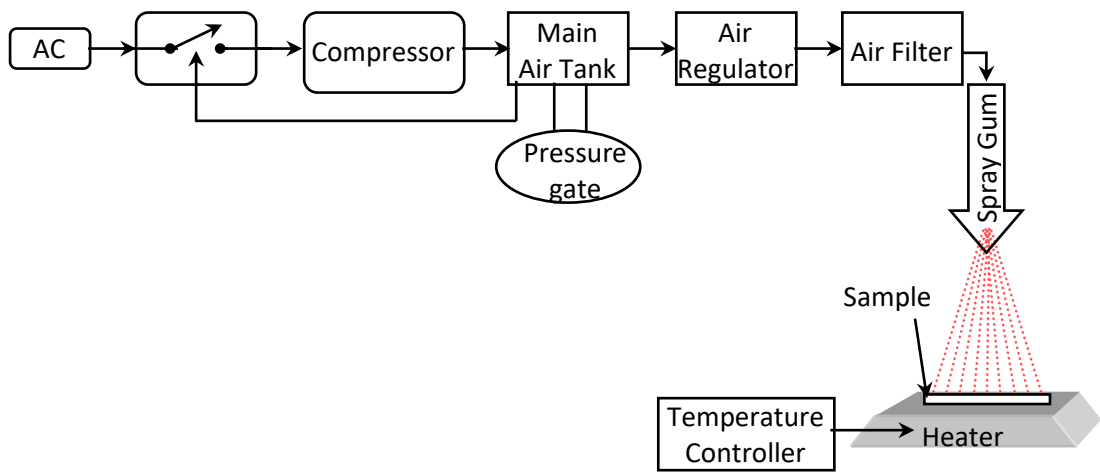
Figure 3.8 Schematic diagram of the spray pyrolysis deposition
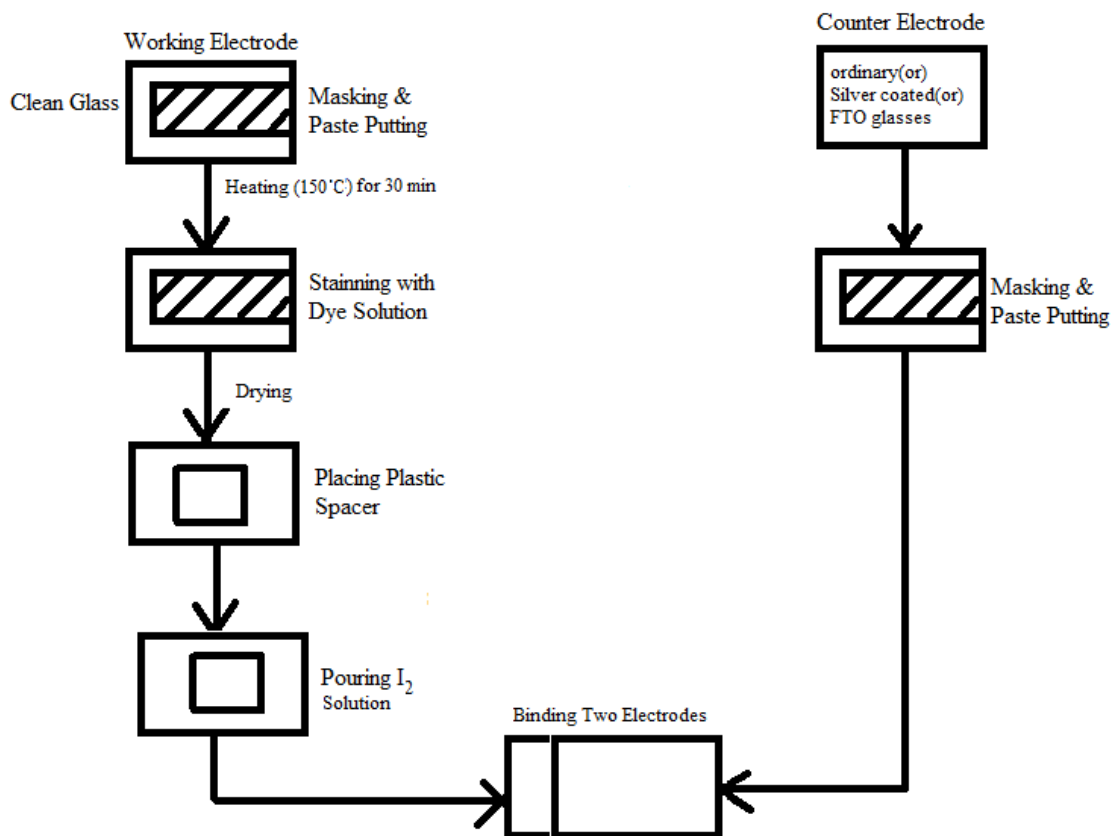
Figure 3.9 The fabrication processes of DSSCs.
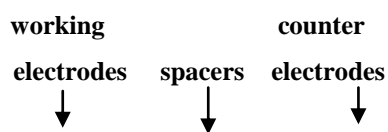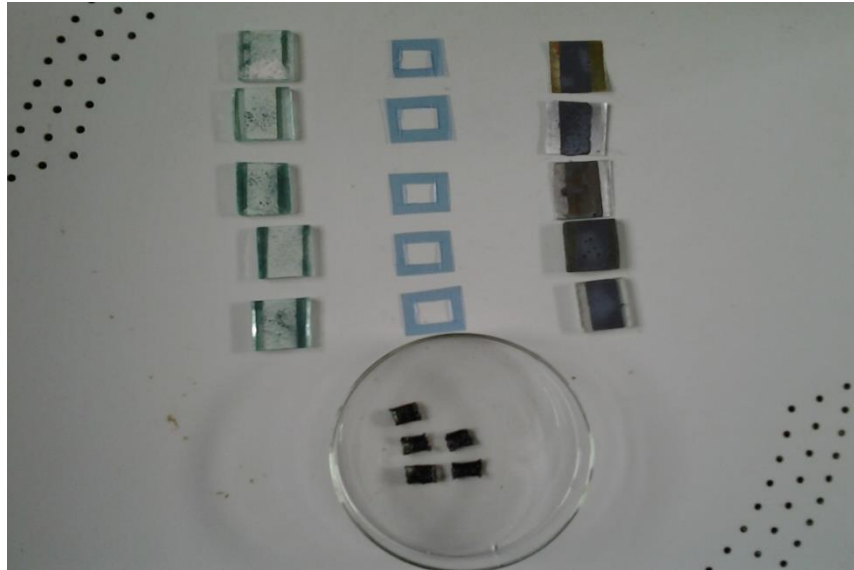
Figure 3.10. The prepared working electrodes, counter electrodes and spacers.
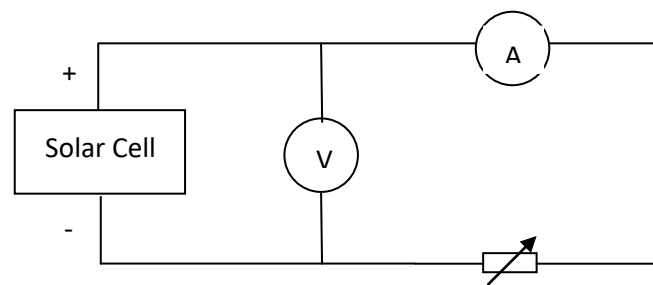
Figure 3.11 The experimental setups for measuring the current-voltage

characteristics of DSSCs.
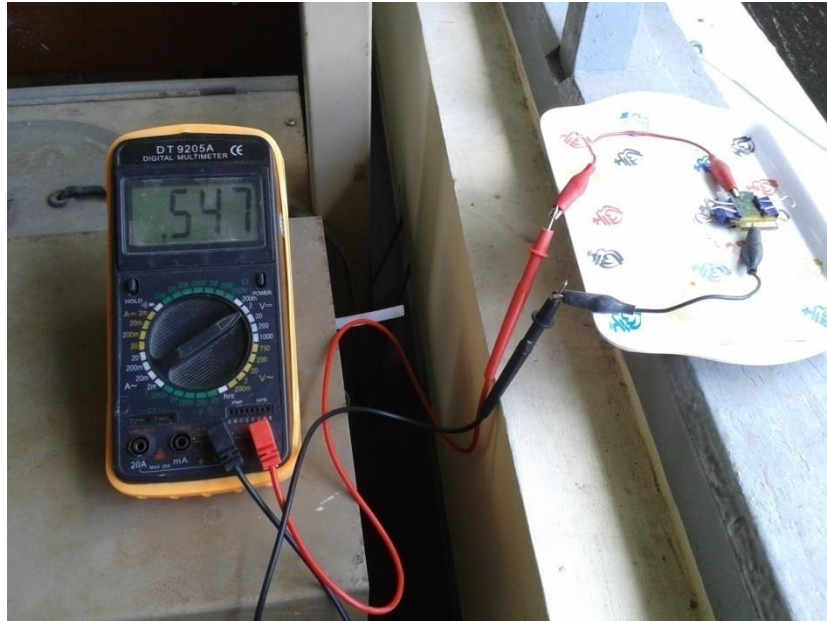
Figure 3.12 The photograph for measuring V_{oc} & I_{sc} in Sunlight.
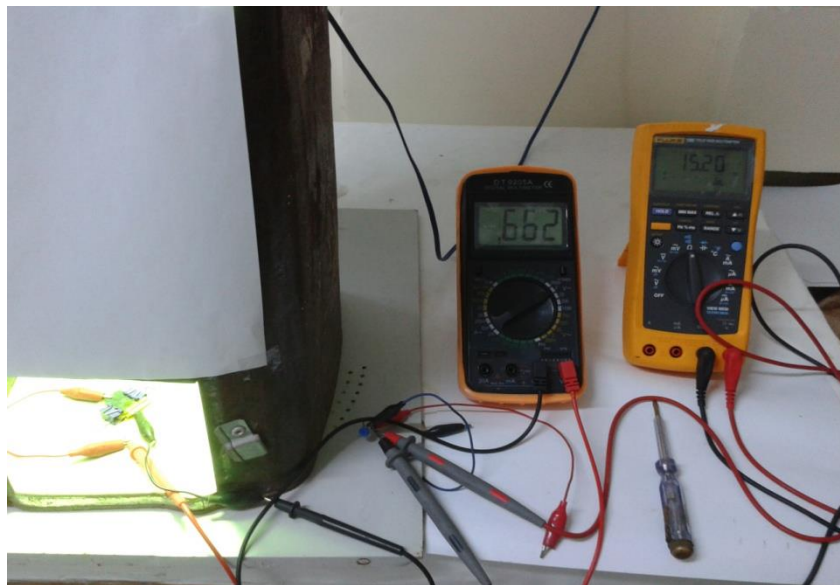
Figure 3.13 The photograph of a DSSC when measuring I-V characteristic under

illumination.
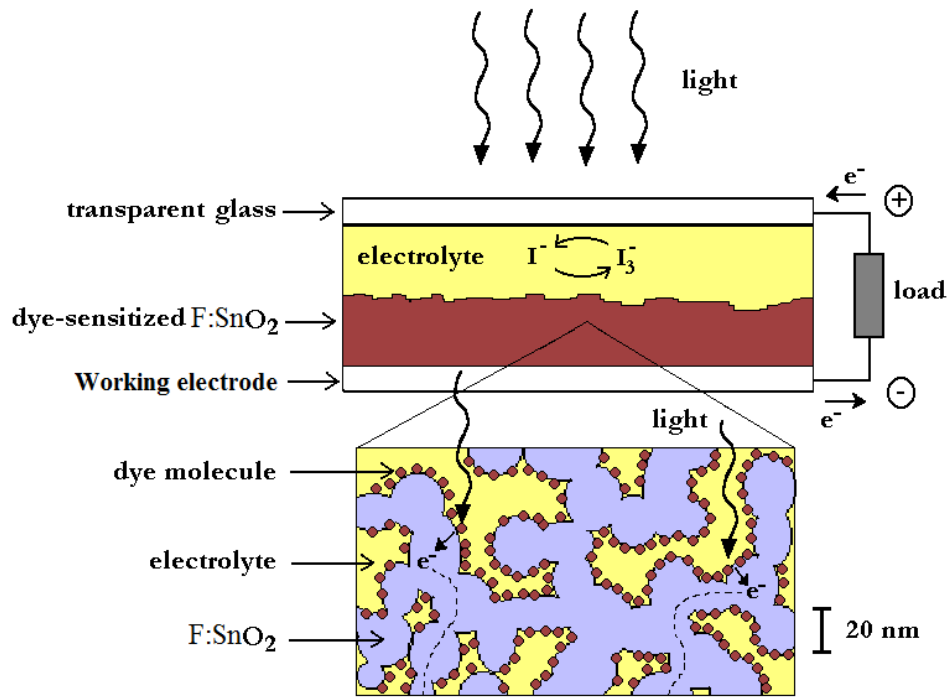
Figure 3.14 The schematic representation of the structure and components of the

dye-sensitized solar cells.
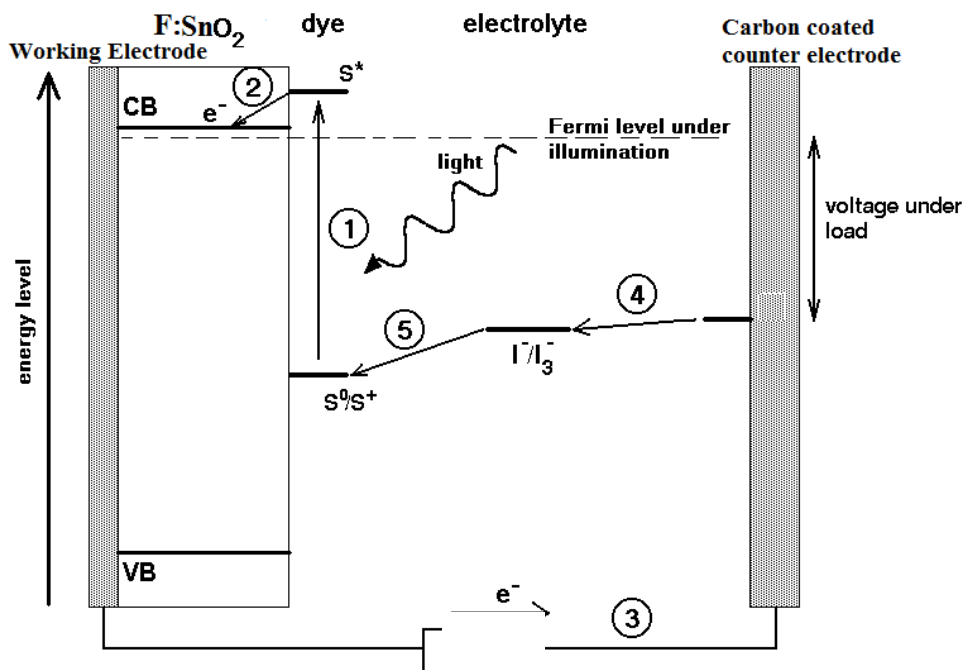
Figure 3.15 The working Principles of DSSCs

CHAPTER IV

RESULTS AND DISCUSSION

4.1 Observation on Fluorine Doped Tin Oxide (F:SnO$_2$) Powder

The phase formation of F: SnO$_2$ powder is analyzed by X-ray diffraction (XRD) method. XRD patterns of nanoporous F: SnO$_2$ samples are shown in Figures 4.1, 4.2 and 4.3. Variation of 2 θ, d-spacing and FWHM with annealing temperature is listed in Table 4.1.Crystallite size (g) and lattice parameter (a) is listed in Table 4.2. According to XRD results, it can be concluded that the annealing temperature can increase crystallization and growing of F: SnO$_2$ nanocrystallite. The preferred orientation indicates (1 1 0), (1 0 1), (2 1 1) for SnO$_2$ and (2 0 0) for fluorine, respectively.

The surface morphology of the F:SnO$_2$ samples has been characterized by Scanning Electron Microscopy (JEOL-JSM 5610LV). The SEM photographs of F doped SnO$_2$ sample at 550 °C, 650°C and 750°C are shown in Figure 4.4, 4.5 and 4.6 respectively. Each photograph exhibits a typical porous structure with many intergrain pores. It is observed that the intergranular pores are linked through the large pores. The pore structure should be regarded as interconnected voids that form a kind of capillary tubes. This structure is preferable for the adsorption of dye solution capable of making photo excitation (pumping out of photo electrons). In the micrograph of F: SnO$_2$ sintered at 550°C, the grains are spread out and the mean pore size is about 7nm. After sintering at 750°C, the grains are adhered and the large pores are formed between groups of grains. The mean pore diameter is 7-20nm. The variation of mean pore size of F: SnO$_2$ sample with sintered temperature is shown in Table 4.3.

From UV-Vis Spectroscopy, it was noticed that F:SnO$_2$ powder has lower absorbance value(<1) and wider band gap value(4.11eV-5.31eV). Therefore it can be used as electron transport mediator semiconductor at working electrode of DSSCs. The VU-Vis spectrum of pure and doped SnO$_2$ powder is shown in Figure 4.7.The estimated band gap values and the corresponding wavelengths are listed in Table 4.4. The band gap values are calculated by E$_g$ = 1240/λ.

4.2 Observation on Fluorine Doped Tin Oxide (FTO) Coating Films

The rheological properties of the precursor solution and the structural, optical and electrical properties of the prepared films were observed as the following.

4.2.1 Rheological Properties of the Precursor Solution for FTO Coating

The viscosity variation of the sol solution with aging time, for the sol prepared with the dopant concentration F/Sn ratio 7.5 wt%, at room temperature is shown in Figure (4.8) which indicates a little increase in viscosity up to the aging period of first three days , the viscosity break off the base line termed as break off point and saturated on the six day called the saturation point.

 In spin coating technique,if the films were developed by using the gel aged lower than its break-off point, then spreading and as a result the evaporation precess was also rapid, which causes non-uniformity in film thickness. In contrast, if the films were coated with solution of above saturation point, the quantity of the sol-gel is mostly thrown away from the substrate due to poor adherence and also causes comet formation on the as-coated film. Between 3 and 5 days of aging, good and uniform coating could be obtained. Thus, in this research, the optimum coating period of the sol solution for spin coating is fixed between 3 and 5 days.

In Spray Pyorolysis Deposition (SPD) technique, if the films wer developed by using the solution higher than its break-off point, the solution will not pass through the nozzle and cannot spread out on the substrate smoothly. Thus in this research the solution was used before break-off point for SPD coating.

4.2.2 Structural Properties of the Films

The XRD pattern of FTO film (developed by spincoating) before post heat-treated is shown in Figure 4.9. The XRD pattern of FTO film (developed by SPD coating) heat treated at 600°C is shown in Figure 4.10. The XRD patterns of FTO thin films (developed by spin coating) heat treated at different

temperatures 325°C, 350°C, 375°C, 400°C, 425°C, 450°C are shown in Figure 4.11. All films have polycrystalline tetragonal rutile structure with lower crystallineity. The average lattice constant a and c are 4.7448Å and 3.1776Å for the film heat treated at 375°C. The film thicknesses were measured by ellipsometer. It was found that the thickness of the films is between 16.8nm to 21.7nm depending on spin coating times of 5 to 9 times. For SPD coating the film thickness is 50-100 nm depending on spray times.

4.2.3 Optical Properties of the Films

The optical properties of prepared films were studied by ellipsometer and UV-Vis spectrometer. The refractive indexes of the films are varied according to treated temperature of the film and wavelength of the incident light. e.g. the refractive indices of the film heated at 375°C are 1.2054 for 607nm and 1.4769 for 312nm of incident light. The experimental data of Ψ Vs λ for the film heat treated at 375°C is shown in Figure 4.12.The transmittance spectra of the films (developed by spin coating) according to heating temperatures are shown in Figure 4.13. It was noticed that the transmittance of the prepared films decreases with the increasing temperature.

The direct band gap energy evaluated from the optical absorption data lies between 3.25 eV and 3.85eV. The plot of $(\alpha h\nu)^2$ Vs hν for spin coating is shown in Figure 4.14 and that for SPD is shown in Figure 4.15. Since the prepared films have lower transmittance and wider band gap value, it is suitable to be used as window conducting electrode in DSSCs' fabrication.

4.2.4 Electrical Properties of the Films

The sheet resistances of the prepared films developed by spin coating and SPD coating were listed in Table 4.5 and 4.6 respectively. From these result it can be noticed that the film resistance depends on the post heated temperature in spin coating and substrate temperature in SPD coating.

4.3 UV-Vis Response of Some Chemical Dyes

The UV-Vis absorption spectra of mercurochrome dye, methyl blue dye and coumarin dye are shown in Figure 4.16, 4.17 and 4.18 respectively. Since they havev the higher absorbance value in visible region, they should be used in DSSCs' fabrication. Since they have lower band gap value, they should be used as sensitizer for DSSCs.

4.4 Measurement of Parameters of DSSCs

The current voltage characteristic curves and power voltage characteristic curves for fabricated cells were shown in Figures 4.19-4.36.

Figures show the typical shape of the current-voltage curve of a photovoltaic cell. The measured open circuit voltage (V_{OC}) and short circuit current (I_{SC}), the estimated maximum voltage (V_{MPP}) and maximum current (I_m) and the calculated energy conversion efficiency(η) and fill factor (FF)for each cells were listed in table 4.7. In this table, the cell numbers 10,11 and 12 are stated for comparison of the parameters of the cells with and without TCO layers. The energy conversion efficiency (η) can be calculated by equation 4.1.

$$\eta = \frac{MPP}{E \times Ac} \qquad \text{---------- (4.1)}$$

where, E = illumination, A_c = effective cells' area

The Fill factor (FF) can be calculated by equation 2.1.

Table 4.1 Variation of 2θ, d-spacing and FWHM with annealing temperature

Sample	(hkl)	2θ	d(Å)	FWHM
550˚C	(110)	26.676	3.3389	0.326
650 ˚C	(110)	27.139	3.2831	0.546
750 ˚C	(110)	26.498	3.3610	0.641

Table 4.2 Variation of Crystallite size (g) and lattice parameter (a)

Sample	Crystallite Size g (nm)	Lattice Parameter a (Å)
550˚C	24.76	4.72
650 ˚C	14.79	4.64
750 ˚C	12.59	4.75

Table 4.3 Crystallite size (g) and lattice parameter (a)

Temperature (˚C)	Mean pore size (nm)
550	7
650	10
750	12

Table 4.4 Band gap values calculated from respective wavelength values

sample	First scan (200-400)nm		Second scan (190-1100)nm		Mean value E_g (eV)
	λ	E_g(eV)	λ	E_g(eV)	
Pure SnO_2	230	5.31	237	5.23	5.27
F:SnO_2(550˙C)	237	5.23	297	4.175	4.70
F:SnO_2(750˙C)	236	5.24	302	4.106	4.67

Table 4.5. The variation of sheet resistance with the film heat-treated
temperature (film were developed by spin coating).

Heat treated temperature(°C)	Sheet resistance(kΩ)
325	98.6
350	14.7
375	13.3
400	15.8
425	19.2
450	32.9

Table 4.6 The variation of sheet resistance with the film heat treated
temperature (film were developed by Spray Pyorolysis Deposition).

Heat treated temperature(°C)	Sheet resistance(Ω)
500	57
550	45
600	32
650	20

Table 4.7 The measured open circuit voltage V_{oc}& short circuit current I_{sc},
estimated maximum voltage V_{MPP}& maximum current I_{MPP} and
calculated cells' efficiency (η) and fill factor(FF).

Cells No.	Type of Counter Electrode glass	Type of Dye solution	V_{oc} (V)	I_{sc} (mA)	η (%)	V_{MPP} (V)	I_{MPP} (mA)	FF (%)
1	Ordinary	Mercurochrome	0.59	0.13	0.0300	0.50	0.060	39.11
2	Ordinary	Methyl blue	0.55	0.11	0.0263	0.47	0.056	43.50
3	Ordinary	Coumarin	0.52	0.09	0.0210	0.42	0.050	44.87

4	Ordinary+ Metal mesh	Mercurochrome	0.59	0.38	0.1092	0.39	0.280	48.70
5	Ordinary+ Metal mesh	Methyl blue	0.55	0.35	0.0884	0.34	0.260	45.92
6	Ordinary+ Metal mesh	Coumarin	0.52	0.30	0.0713	0.31	0.230	45.71
7	Silver coated	Mercurochrome	0.56	0.25	0.060	0.40	0.150	48.00
8	Silver coated	Methyl blue	0.53	0.22	0.0546	0.42	0.130	46.80
9	Silver coated	Coumarin	0.46	0.21	0.043	0.33	0.130	44.40
10	FTO	Mercurochrome	0.67	1.60	0.405	0.45	0.900	37.78
11	FTO	Methyl blue	0.57	1.06	0.300	0.40	0.750	45.65
12	FTO	Coumarin	0.51	0.90	0.202	0.32	0.630	40.93
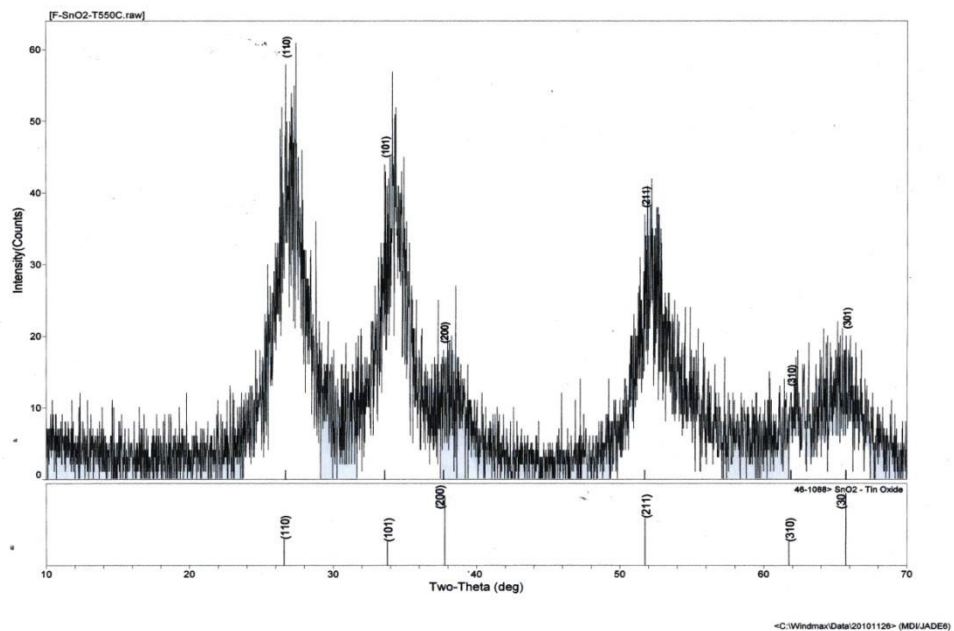
Figure (4.1) XRD pattern of nanoporous F:SnO$_2$ Sample (550°C)
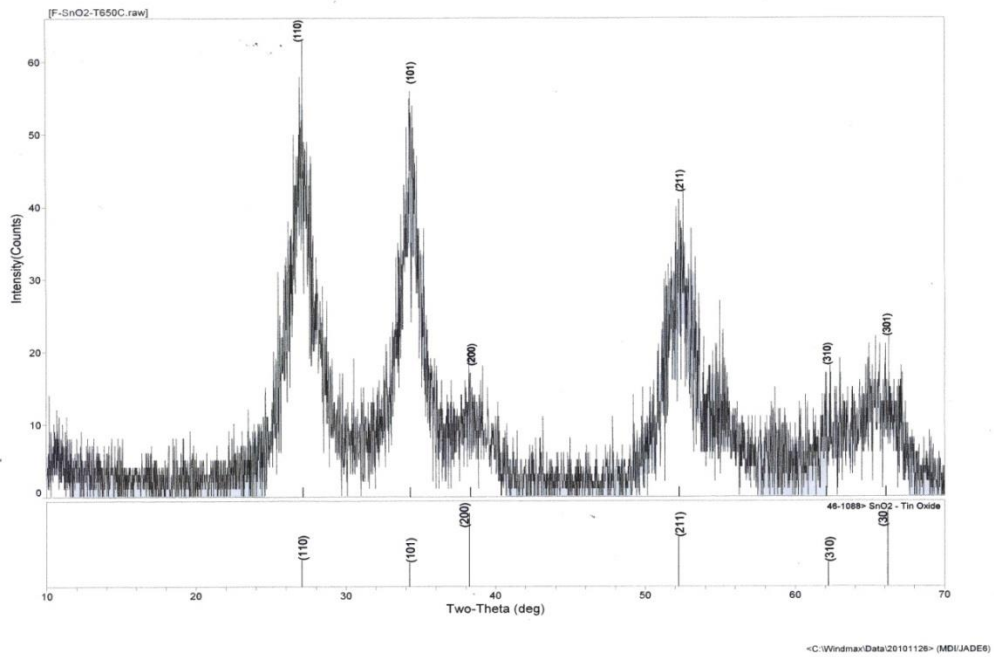
Figure (4.2) XRD pattern of nanoporous F:SnO$_2$ Sample (650°C)
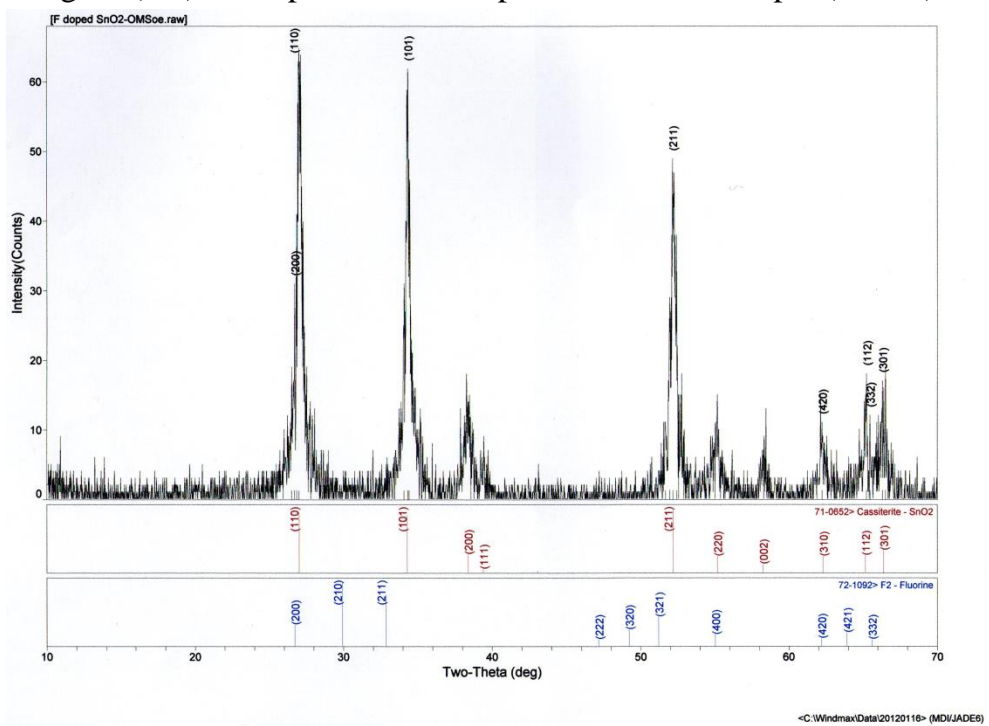
Figure 4.3 XRD pattern of nanoporous F:SnO$_2$ Sample (750°C)
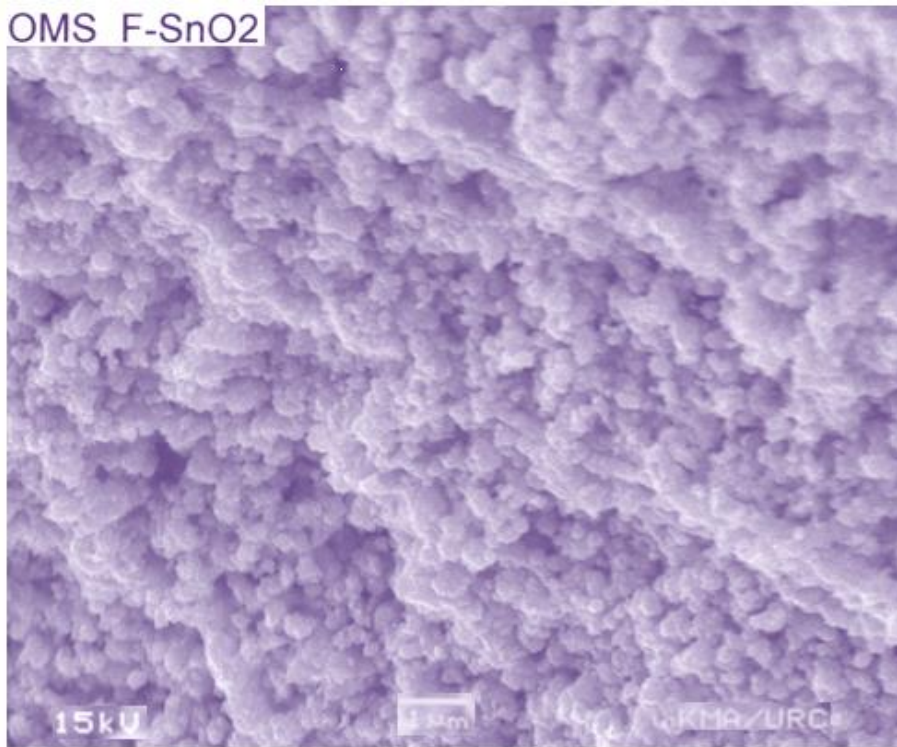
Figure 4.4. SEM photograph of F:SnO_2 Sample (550°C)
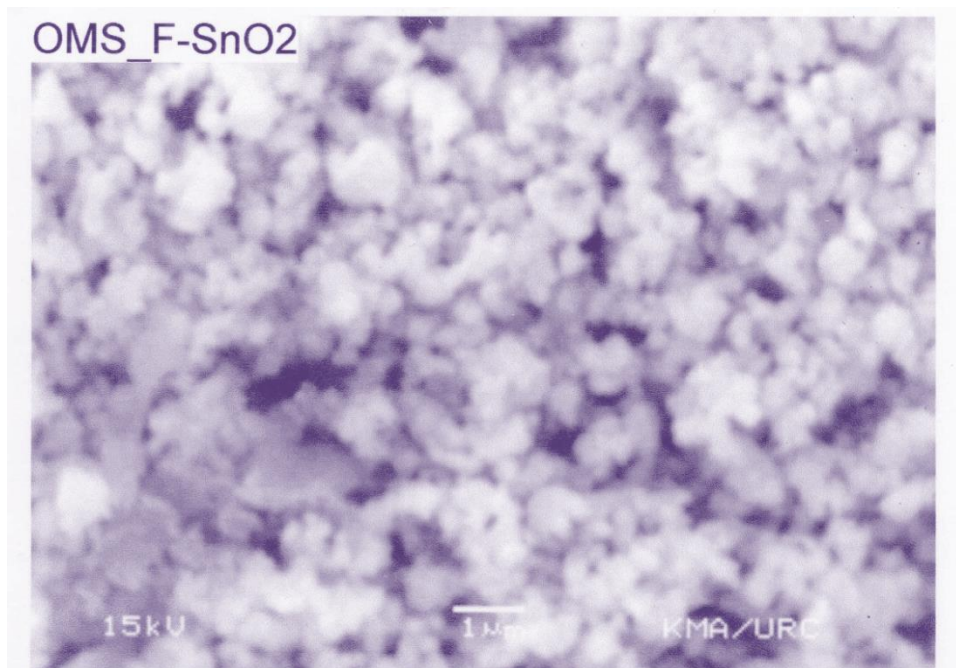
Figure 4.5 SEM photograph of F:SnO_2 Sample (650°C)
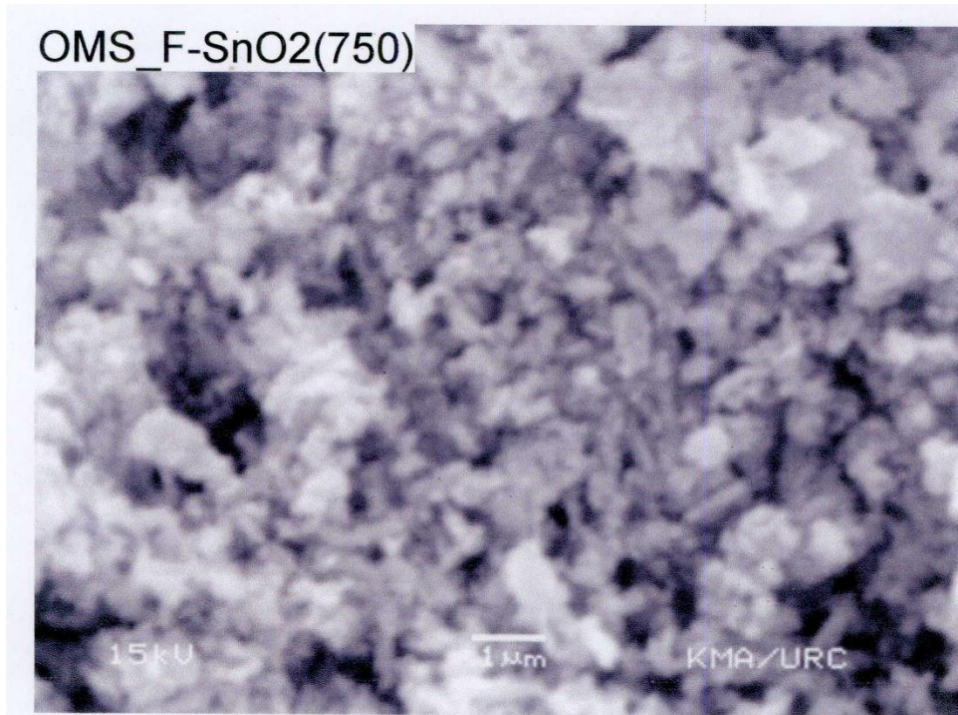
Figure 4.6 SEM photograph of F:SnO$_2$ Sample (750°C)
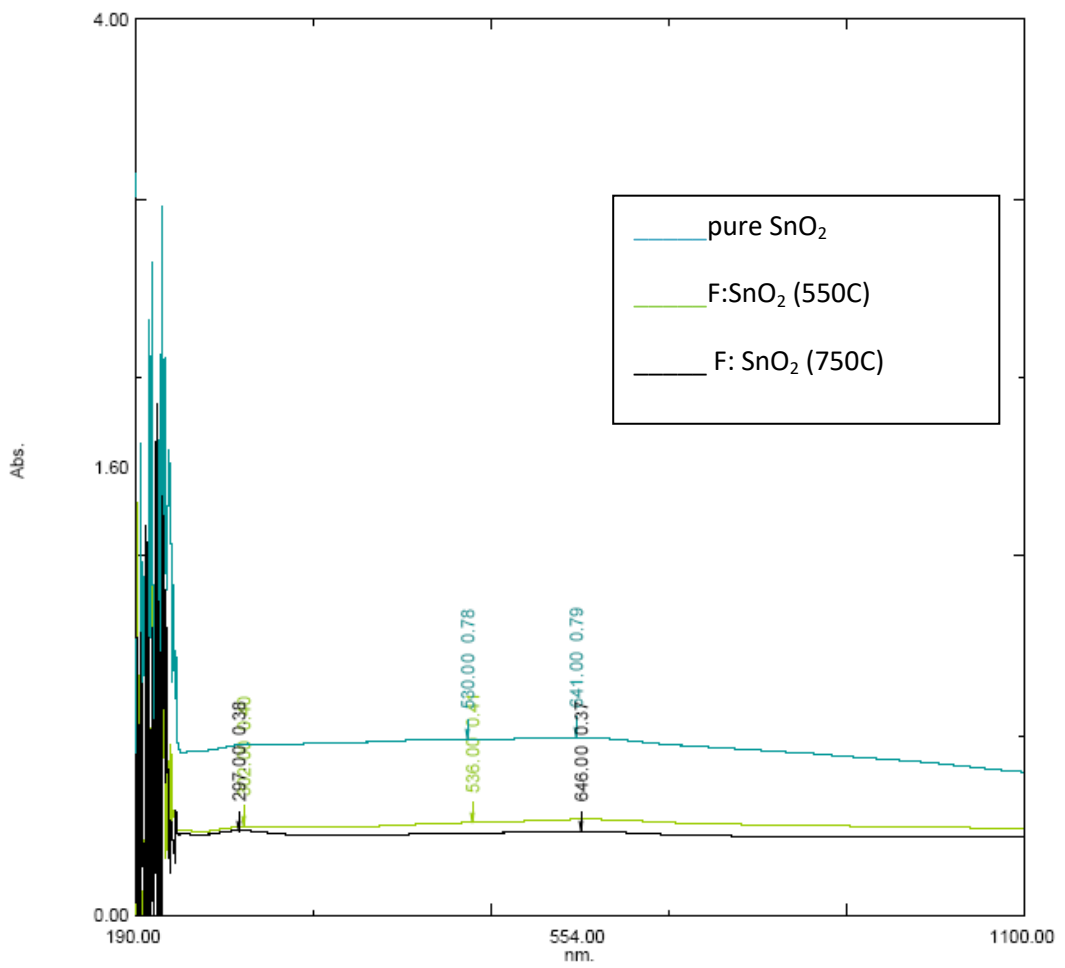
Figure 4.7 UV-Vis spectrum of pure and F doped SnO_2 Samples.
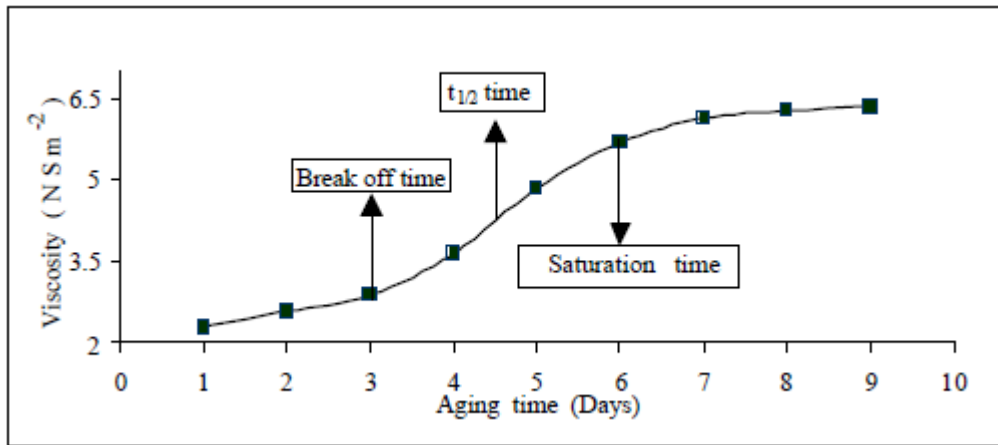
Figure 4.8 The viscosity variation of the sol solution with aging time.
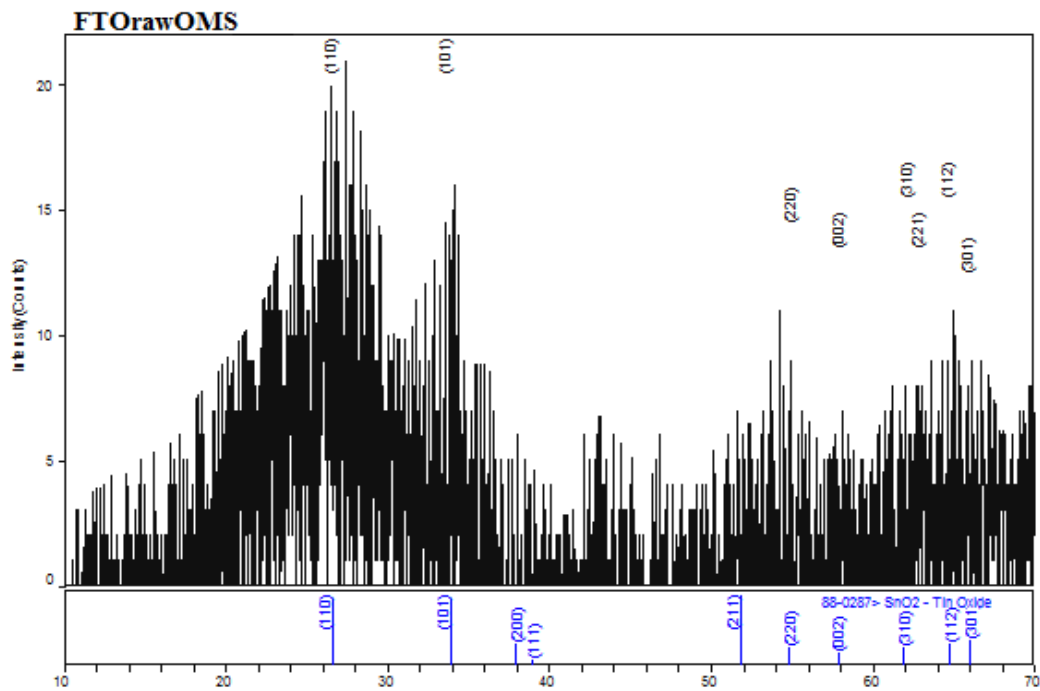
Figure 4.9 The XRD pattern of FTO film developed by spin coating technique

before post heat treated.
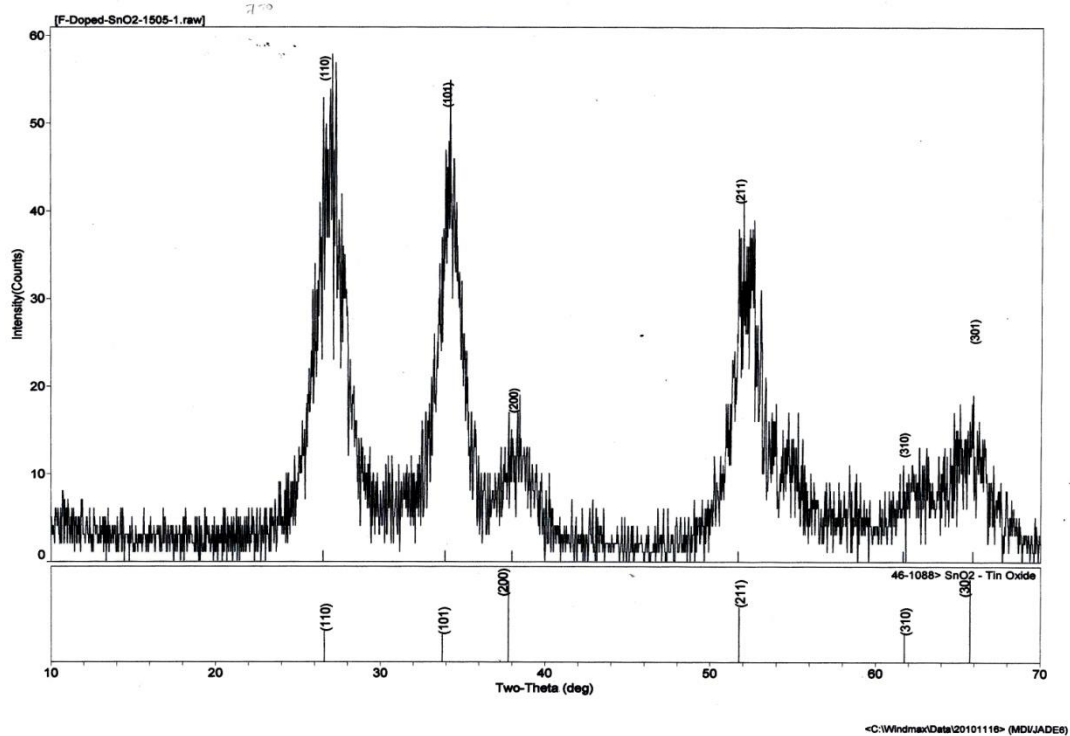
Figure 4.10 The XRD pattern of FTO film developed by SPD coating technique before post heat treated.
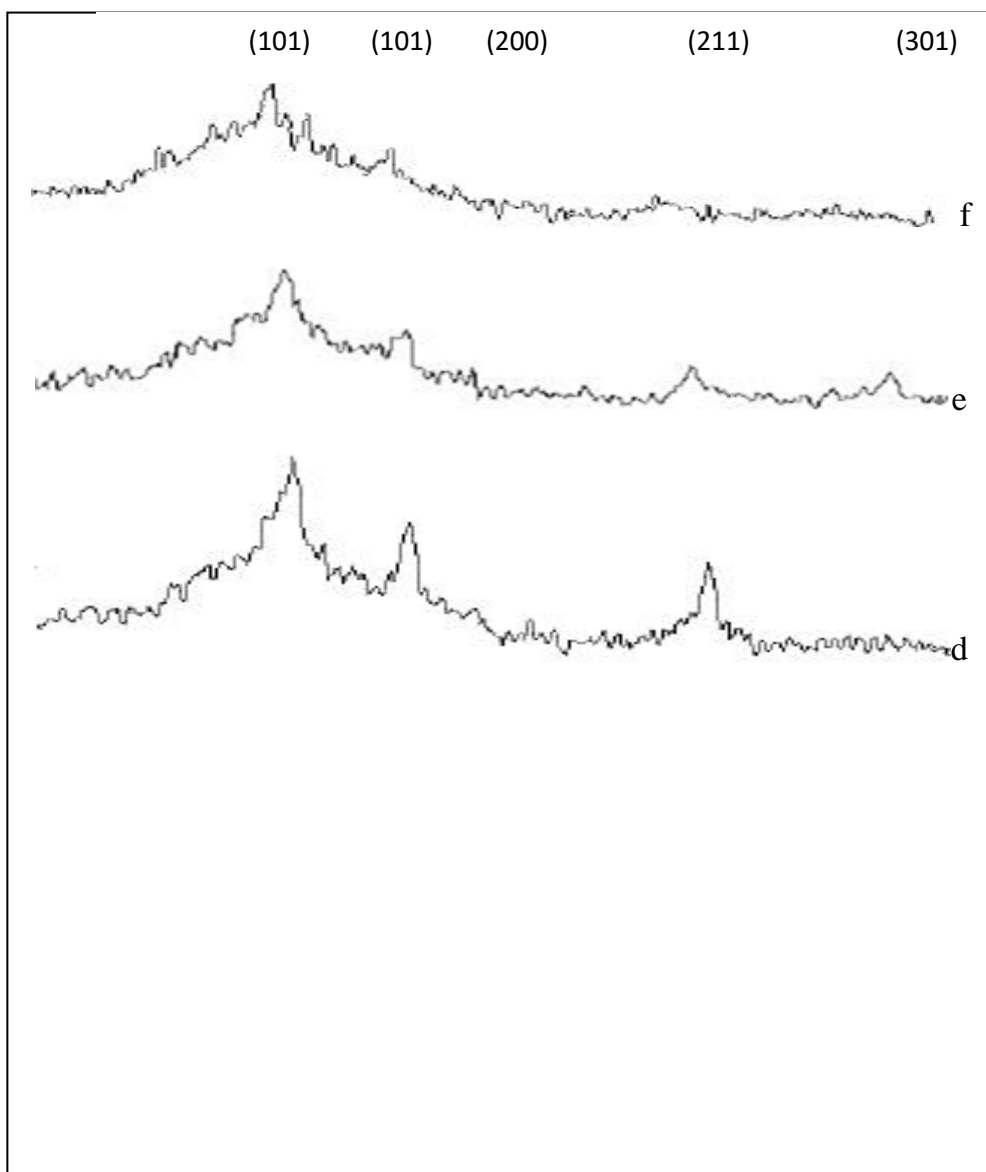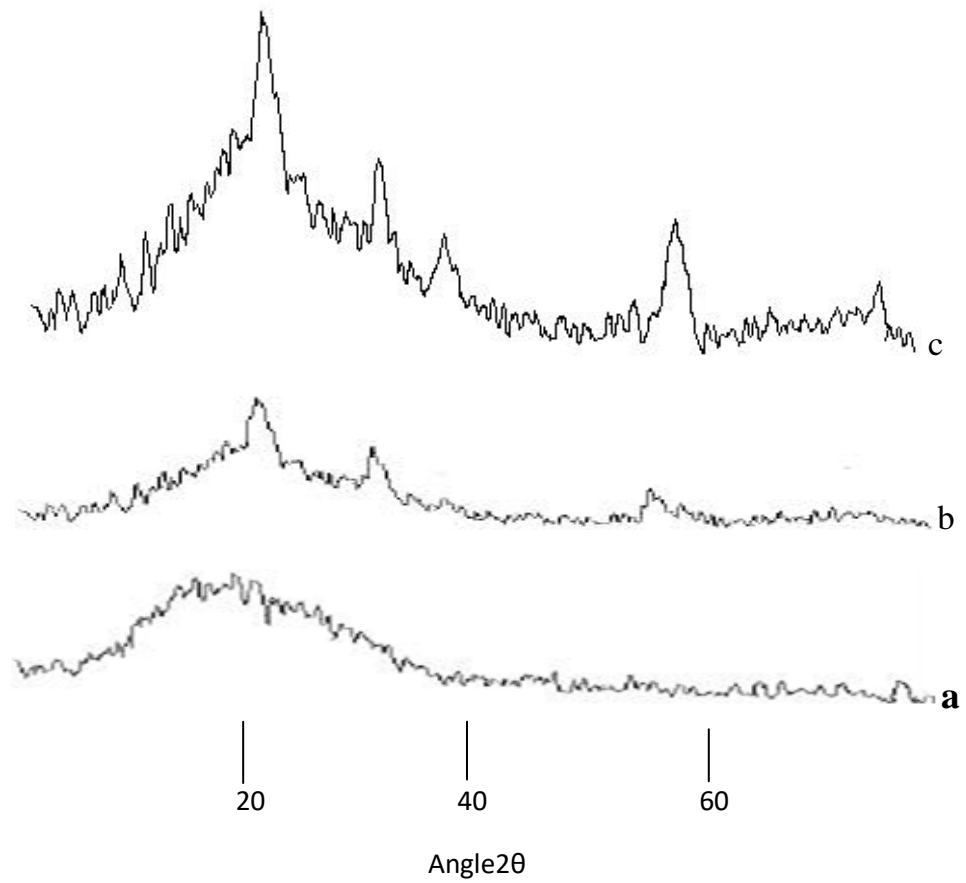
Figure 4.11 The XRD patterns of FTO films heat treated at temperatures (a)325 °C,(b) 350 °C,(c) 375 °C,(d) 400 °C, (e)425 °C, (f)450 °C.
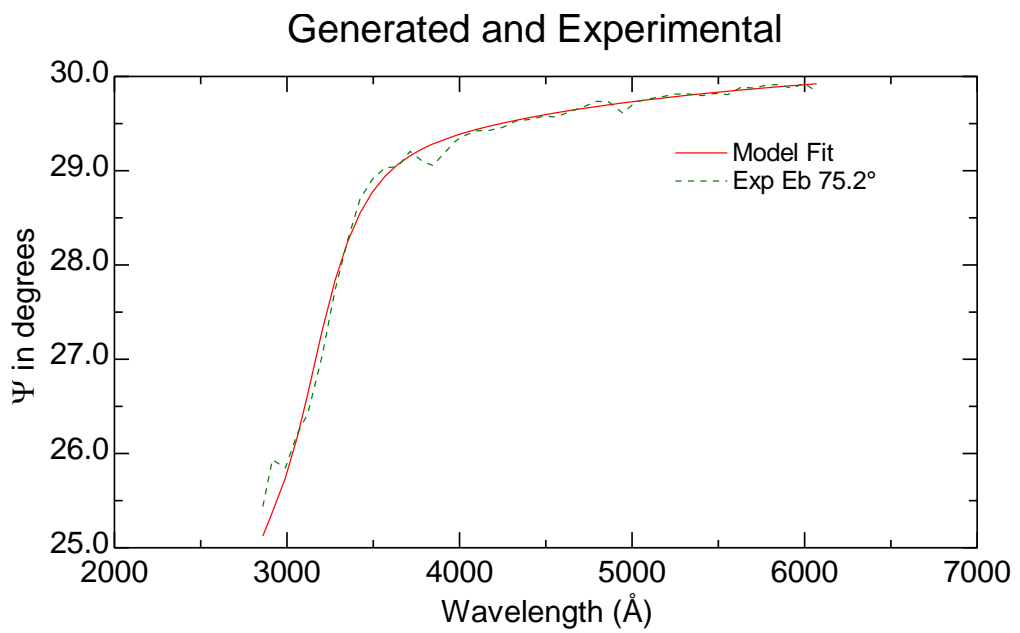
Figure 4.12 The general and experimental data of a FTO film.
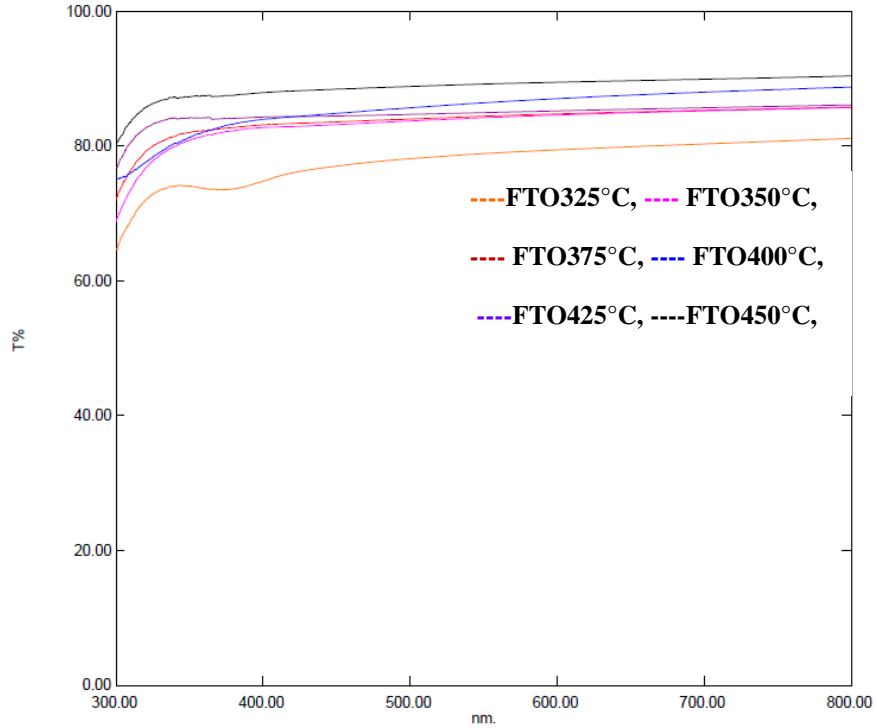
Figure 4.13 The comparison of the Transmittance spectra of FTO films according to the heat treated temperature.
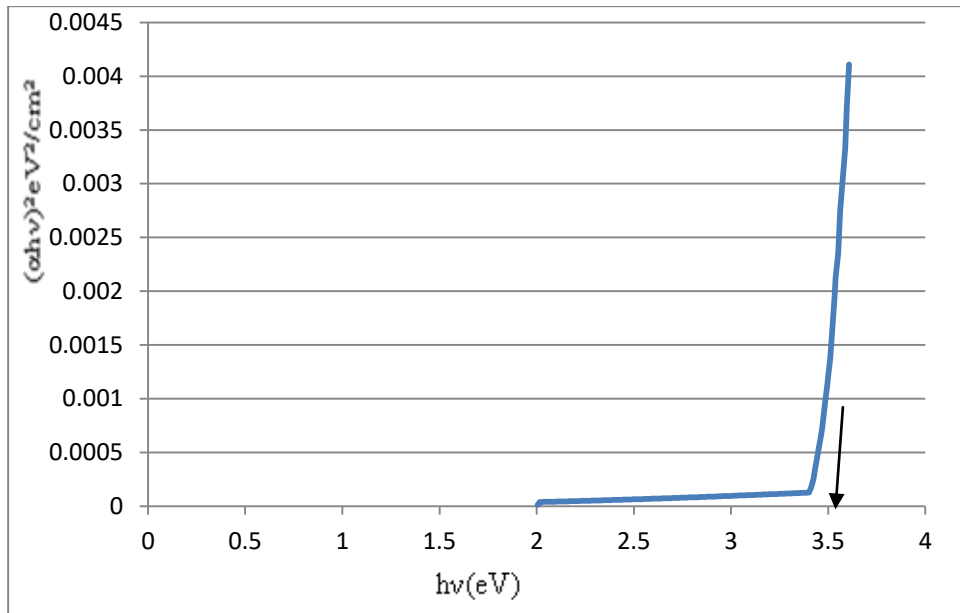
Figure 4.14 Plot of $(\alpha h\upsilon)^2$ Vs $h\upsilon$ for F:SnO$_2$ film developed by spin coating.
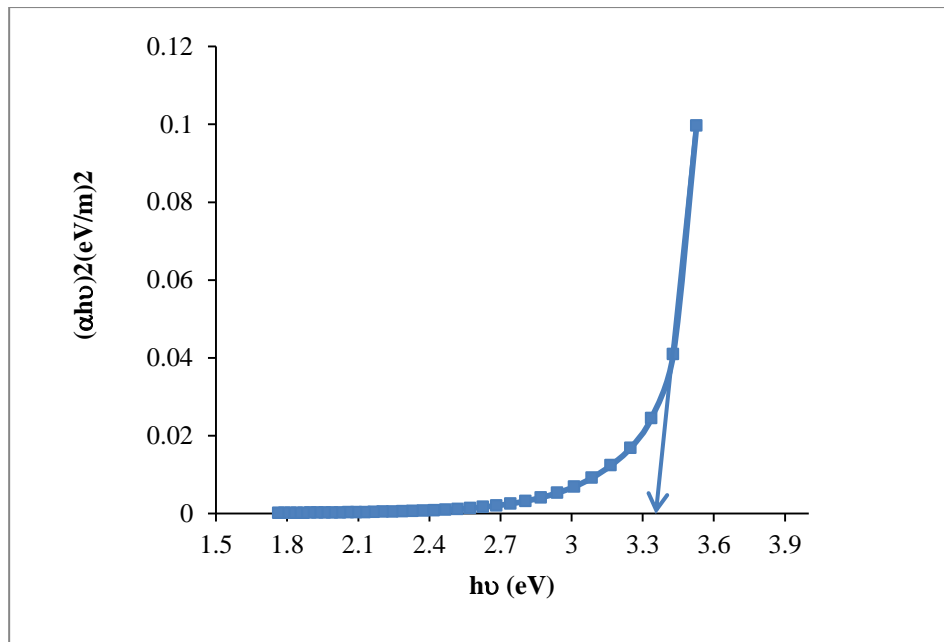
Figure 4.15 Plot of $(\alpha h\upsilon)^2$ Vs $h\upsilon$ for F:SnO$_2$ film developed by SPD coating.
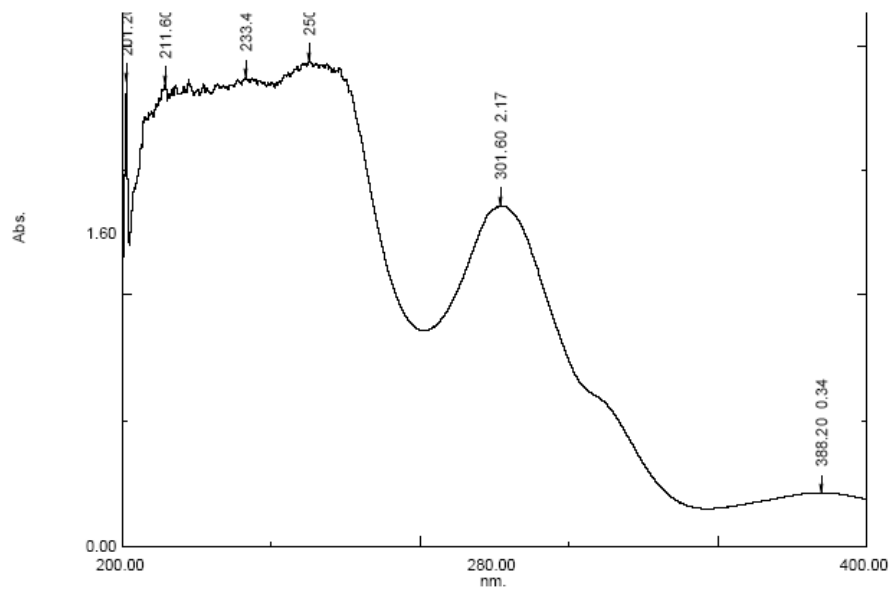
No.	P/V	Wavelength	Abs.	Description
1	⬆	388.20	0.34	
2	⬆	301.60	2.17	
3	⬆	250.40	3.10	
4	⬆	233.40	3.00	
5	⬆	211.60	2.95	
6	⬆	201.20	2.97	
7	⬇	357.40	0.24	
8	⬇	281.20	1.37	
9	⬇	241.00	2.93	
10	⬇	221.00	2.88	
11	⬇	202.00	1.92	

Figure 4.16 UV-Vis spectrum of mercurochrome
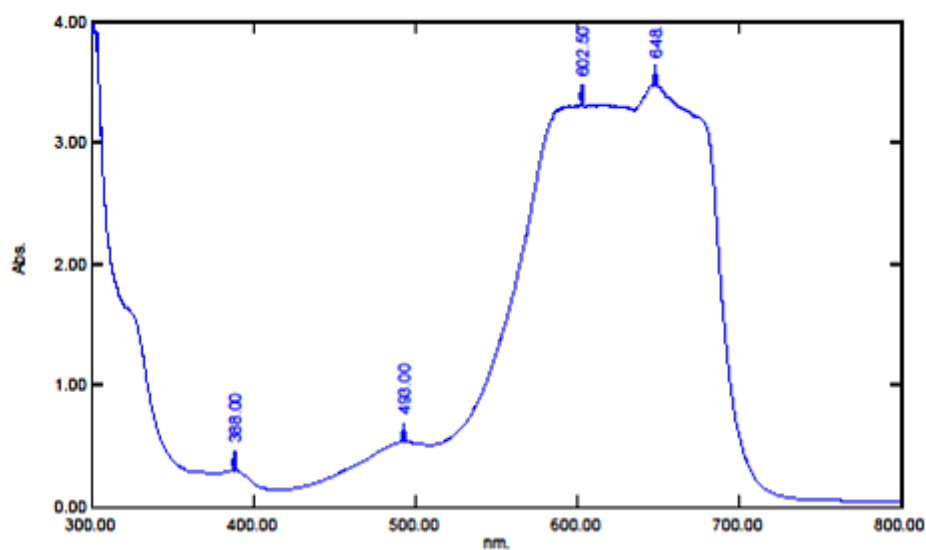
No.	P/V	Wavelength	Abs.	Description
1	⬆	648.50	3.49	
2	⬆	602.50	3.33	
3	⬆	493.00	0.53	
4	⬆	388.00	0.30	
5	⬇	635.00	3.26	
6	⬇	508.00	0.51	
7	⬇	414.50	0.13	
8	⬇	376.00	0.27	

Figure 4.17 UV-Vis spectrum of methyl blue dye
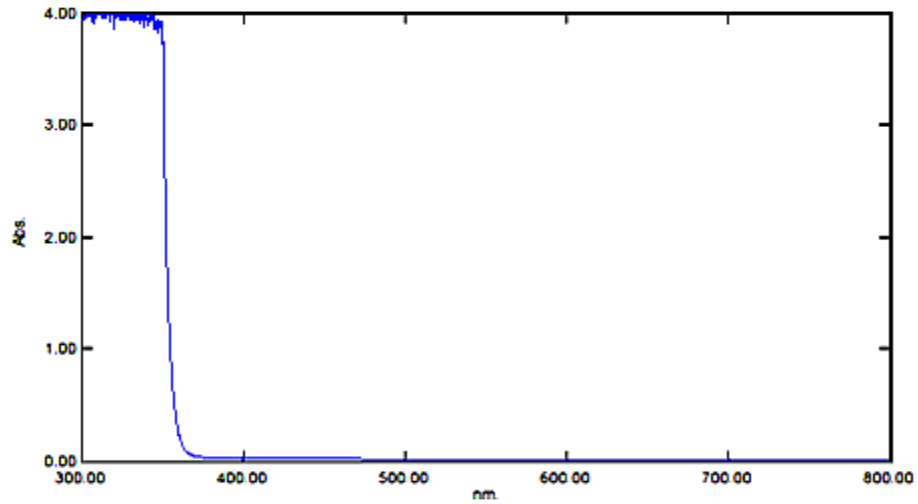
| No.	P/V	Wavelength	Abs.	Description
1	⬆	325.00	4.00	
2	⬆	309.00	4.00	
3	⬇	320.00	3.87	

Figure 14.18 UV-Vis spectrum of Coumarin dye
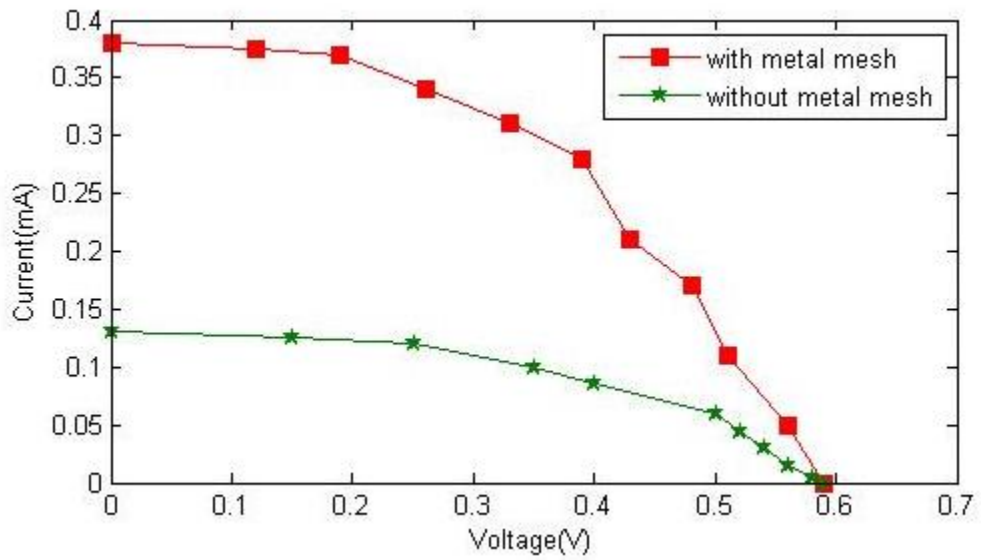
Figure(4.19) I & V Characteristic Curve for DSSC made of Ordinary Glass and Mercurochrome Dye.
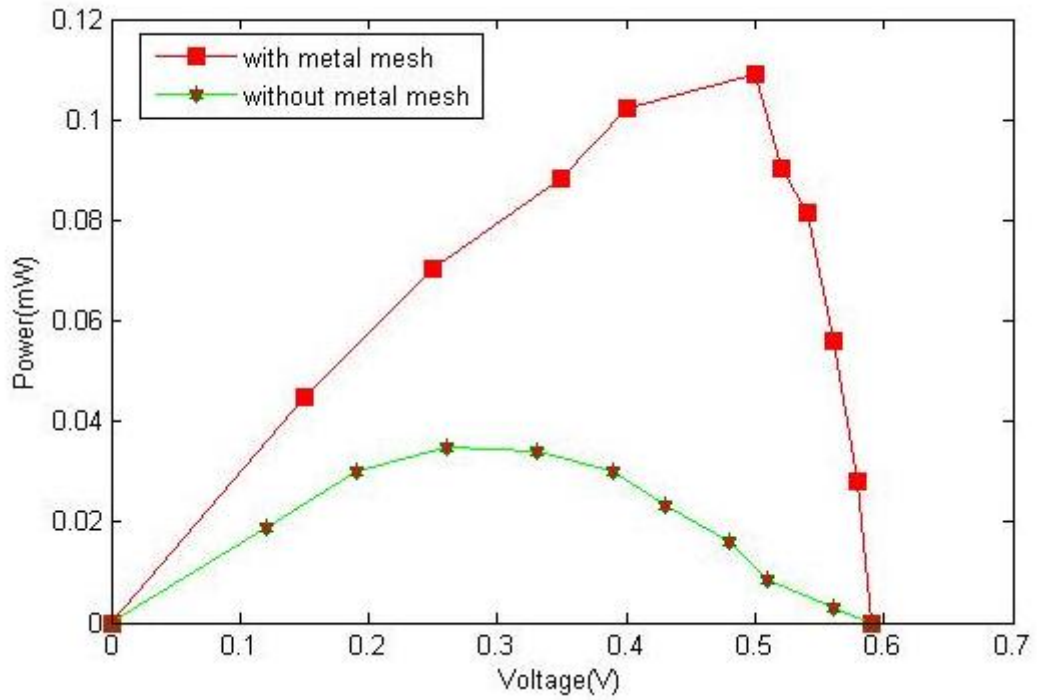
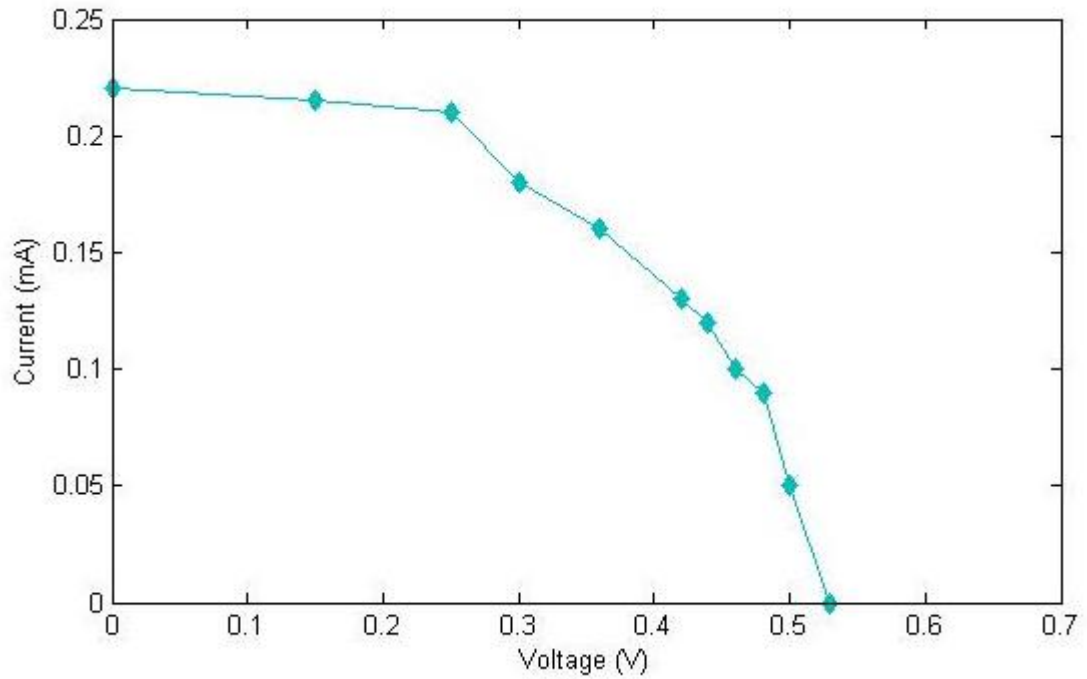Figure (4.20) P & V Characteristic Curve for DSSC made of Ordinary Glass and
Mercurochrome Dye.
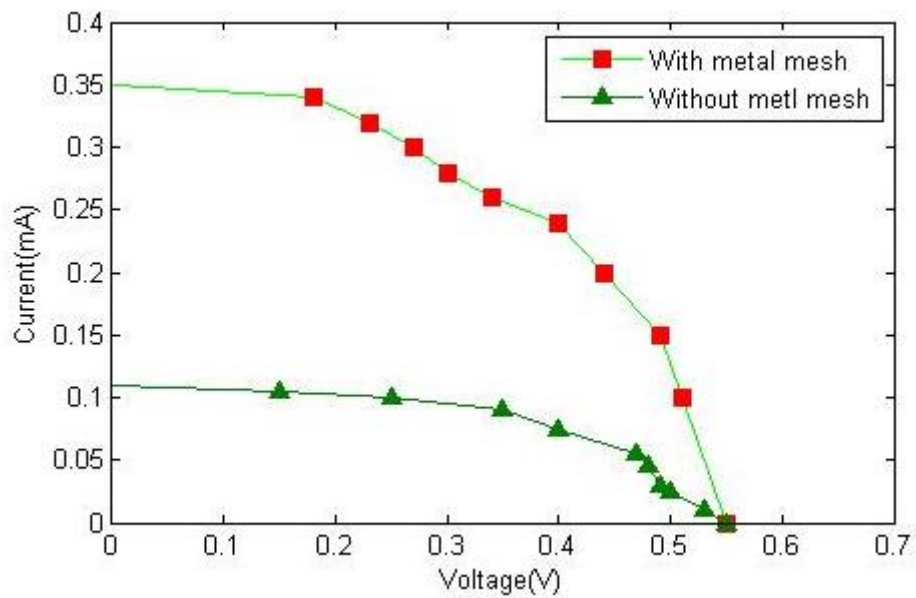
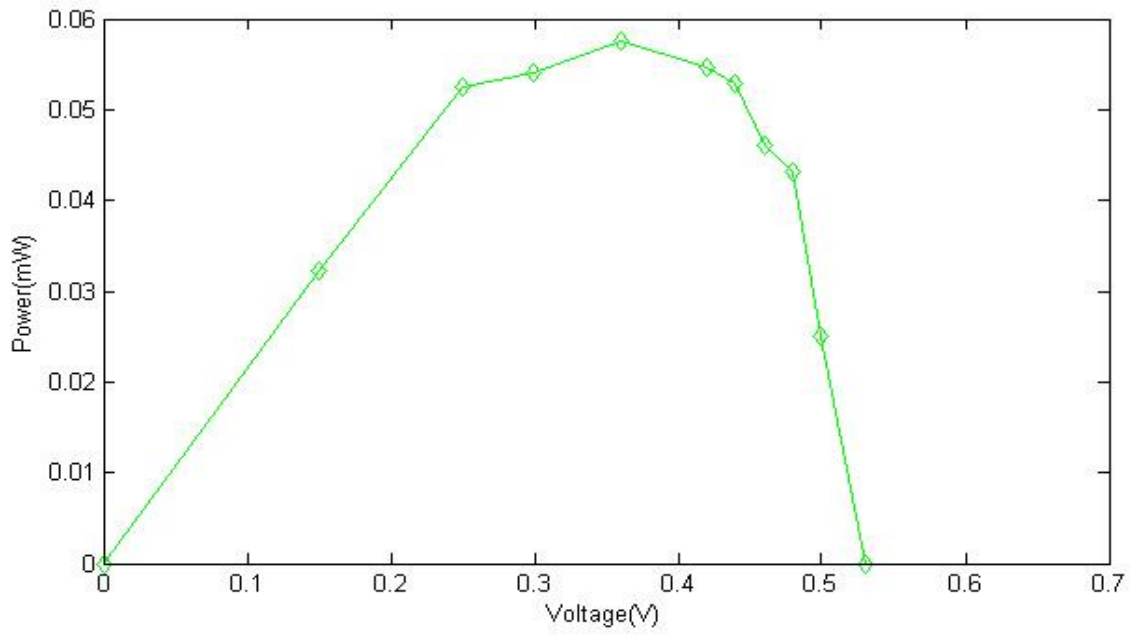Figure (4.21) I & V Characteristic Curve for DSSC made of Ordinary Glass and
Methyl blue Dye.
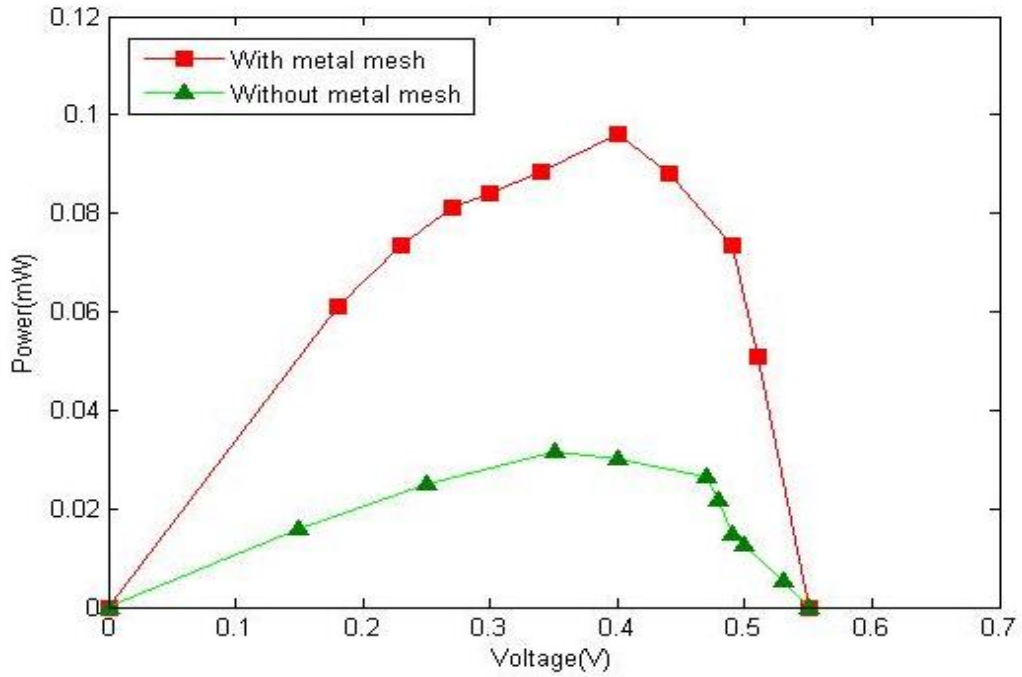
Figure (4.22) P & V Characteristic Curve for DSSC made of Ordinary Glass and

Methyl blue Dye.
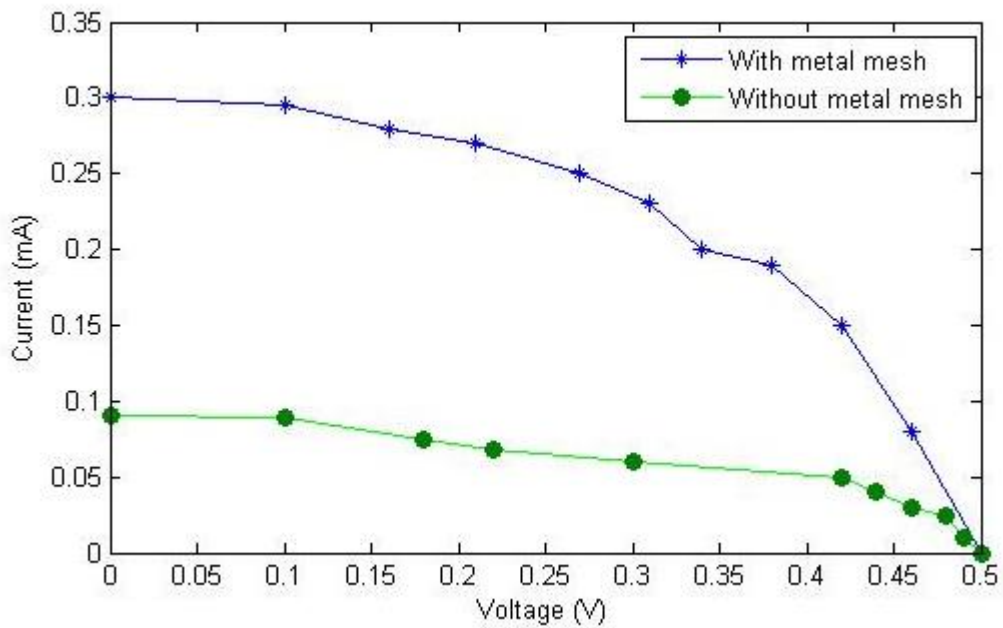
Figure (4.23) I & V Characteristic Curve for DSSC made of Ordinary Glass and Coumarin Dye.
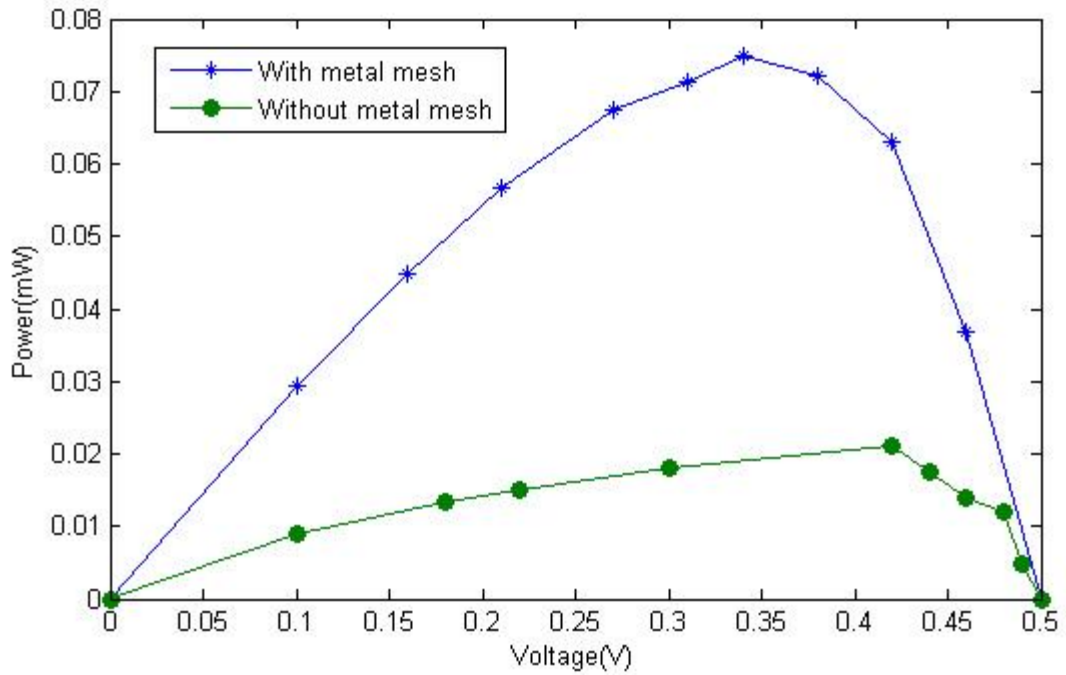
Figure (4.24) P & V Characteristic Curve for DSSC made of Ordinary Glass and

Coumarin Dye.
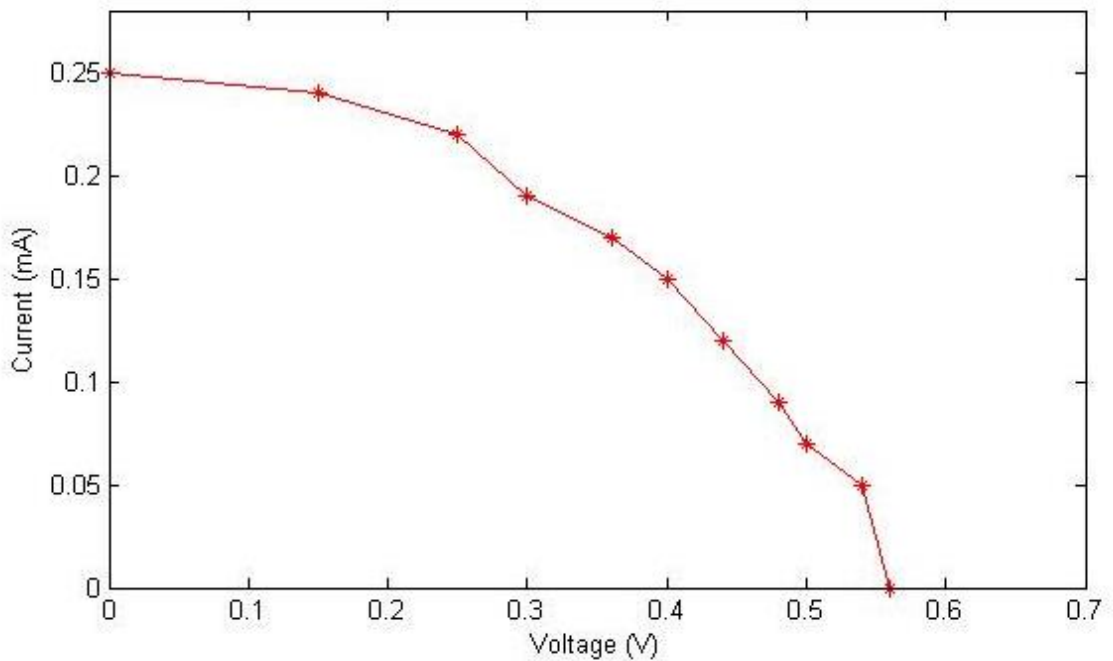
Figure (4. 25) I & V Characteristic Curve for DSSC made of Silver coated Glass
and Mercurochrome Dye.
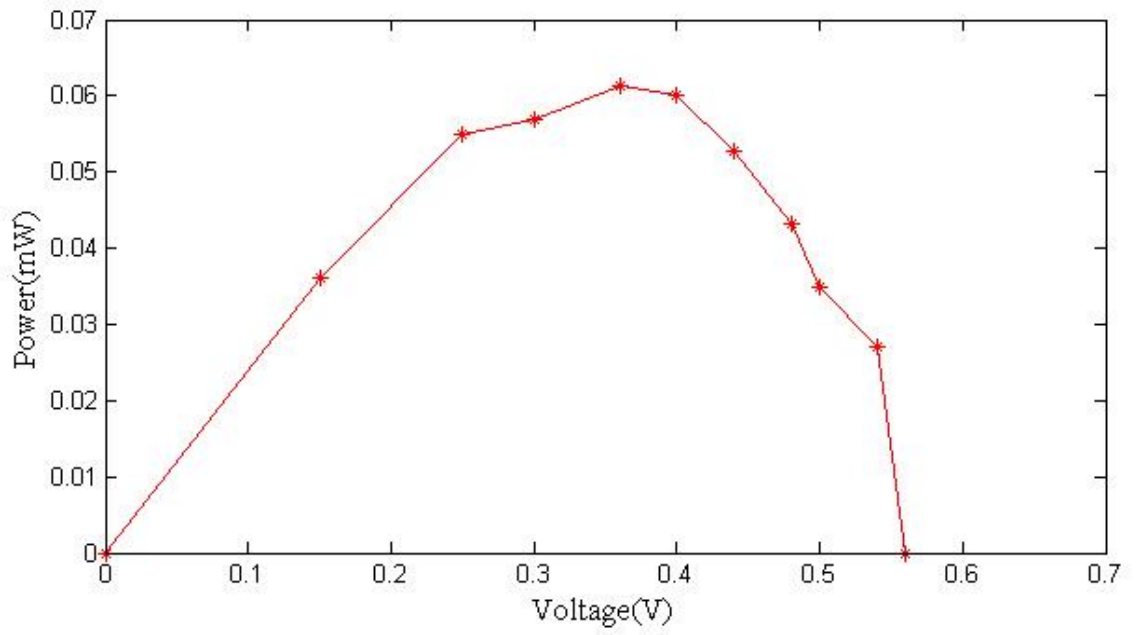
Figure (4.26) P & V Characteristic Curve for DSSC made of Silver coated Glass
and Mercurochrome Dye.

Figure (4.27) I & V Characteristic Curve for DSSC made of Silver coated Glass
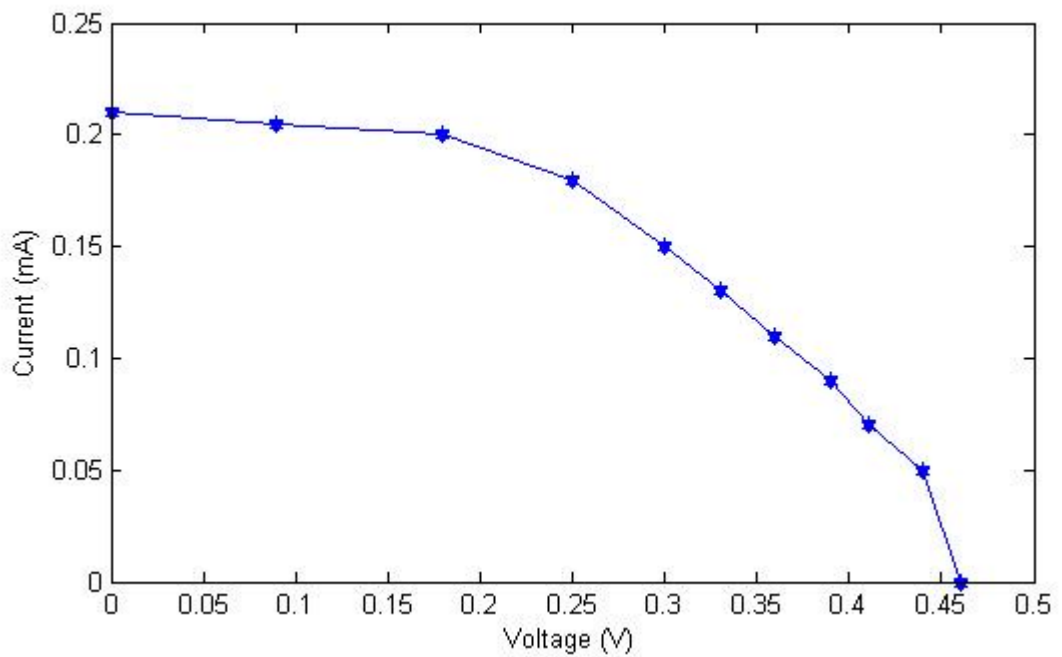and Methyl blue Dye.

Figure (4. 28) P & V Characteristic Curve for DSSC made of Silver coated Glass

and Methyl blue Dye.

Figure (4.29) I & V Characteristic Curve for DSSC made of Silver coated Glass and Coumarin Dye.
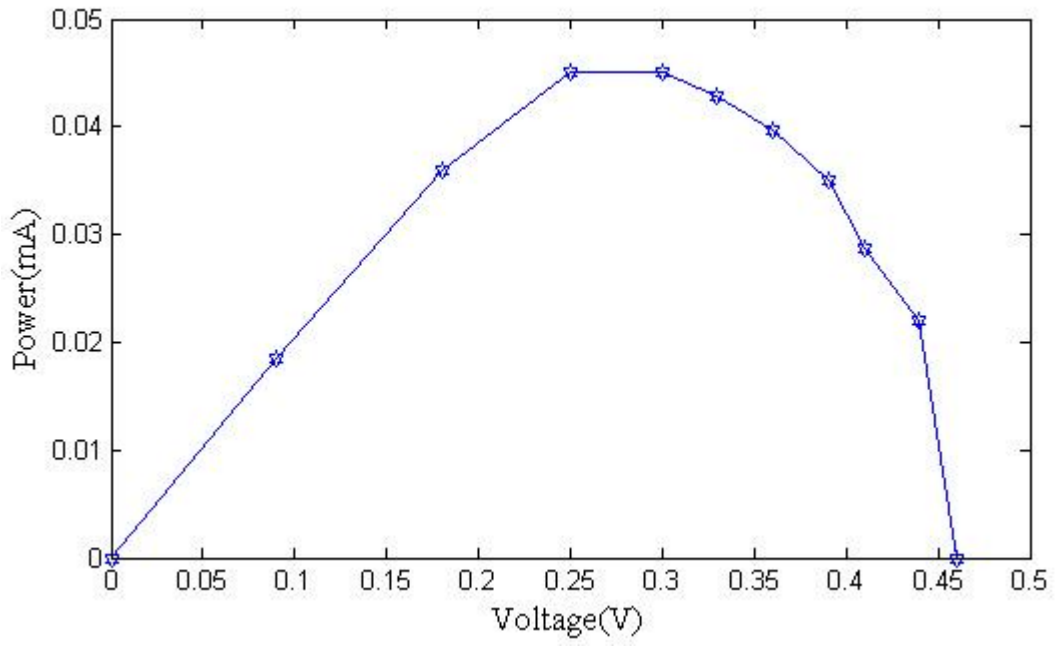
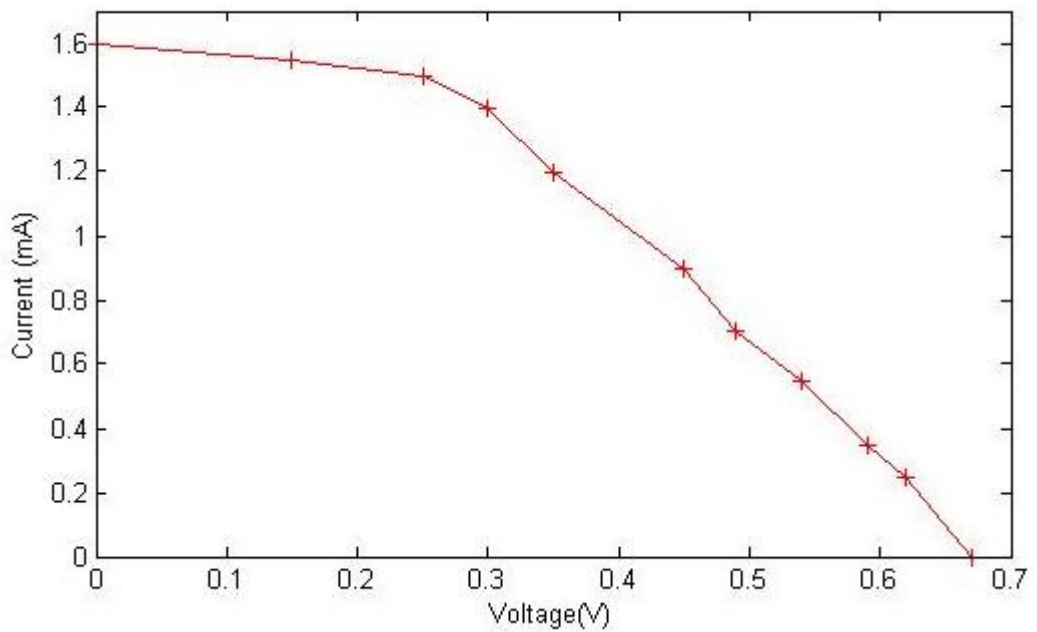Figure (4.30) P & V Characteristic Curve for made of Silver coated Glass and
Coumarin Dye.

Figure (4.31) I & V Characteristic Curve for DSSC made of FTO Glass and
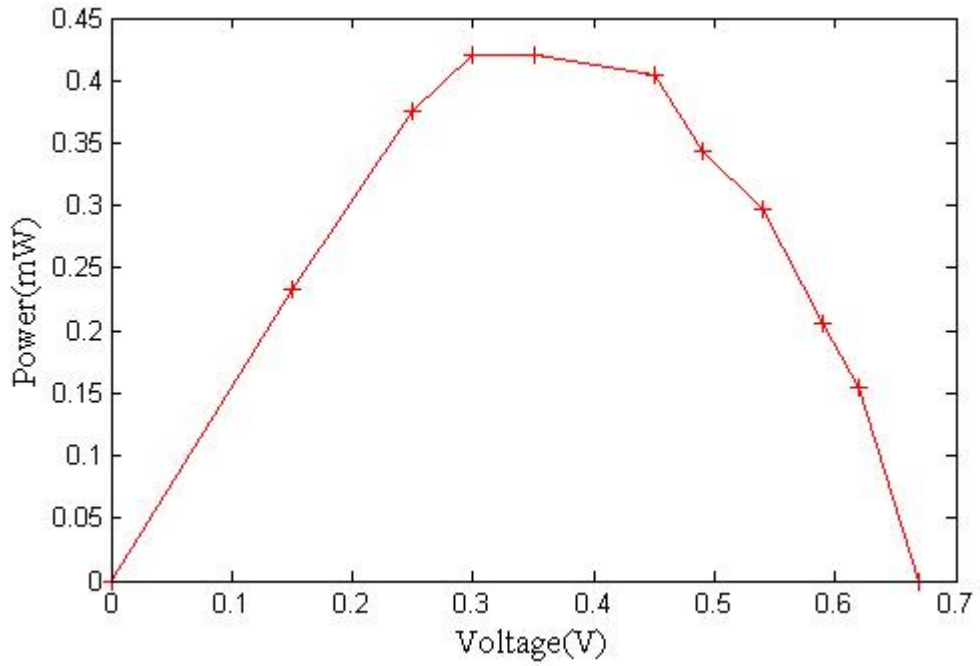Mercurochrome Dye.

Figure (4.32) P & V Characteristic Curve for DSSC made of FTO Glass and Mercurochrome Dye.
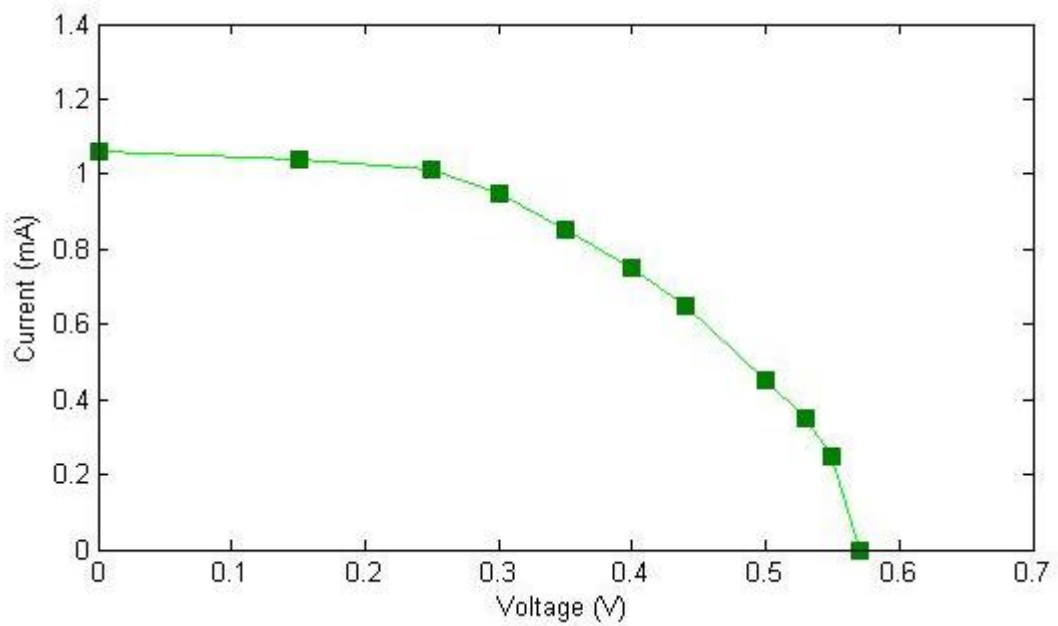

Figure (4.33) I & V Characteristic Curve for DSSC made of FTO Glass and Methyl Blue Dye.
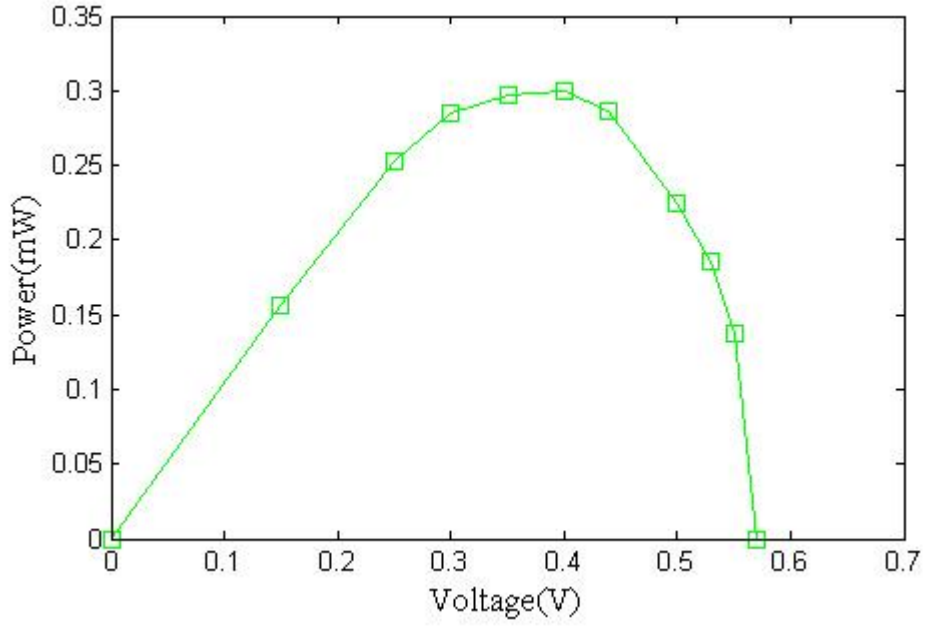
Figure (4.34) P& V Characteristic Curve for DSSC made of FTO Glass and
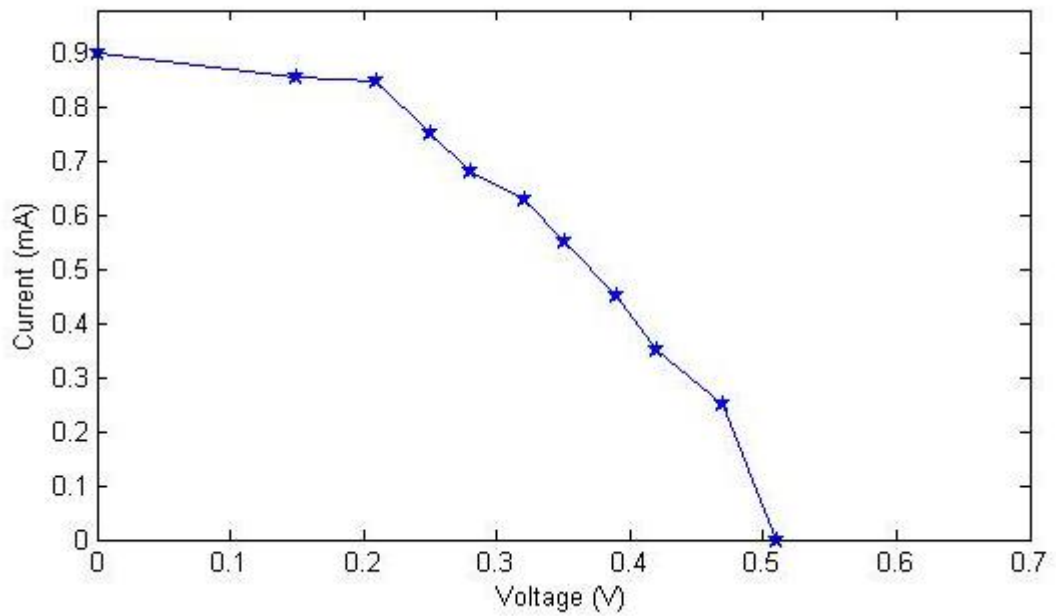Methyl Blue Dye.

Figure (4.35) I & V Characteristic Curve for DSSC made of FTO Glass
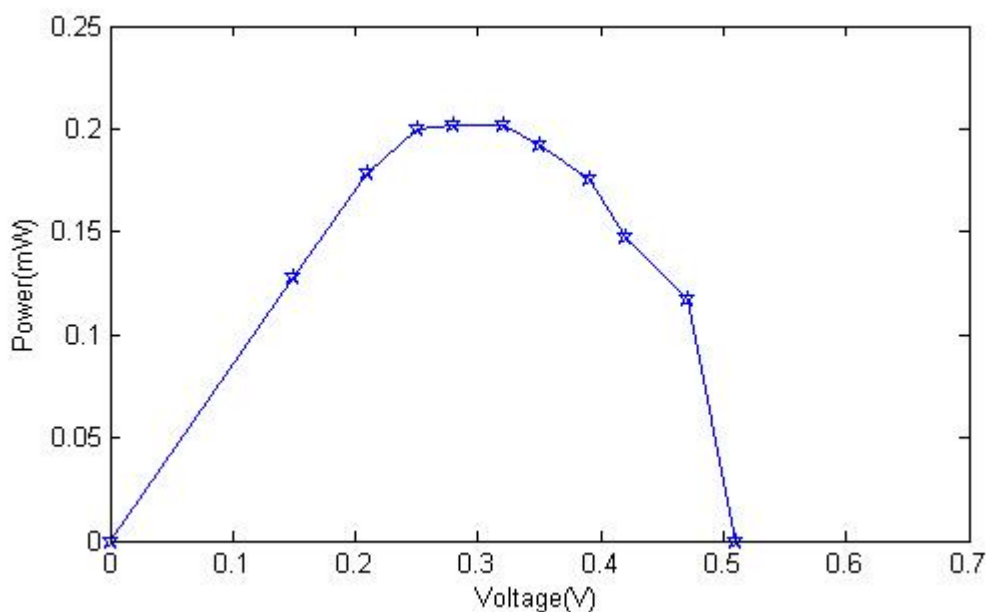and

Coumarin Dye.

Figure (4.36) P & V Characteristic Curve for DSSC made of FTO Glass and
            Coumarin Dye

CHAPTER V
CONCLUSION

The auto-combustion assisted sol-gel method has been proven as synthesis route for F doped SnO_2 powder. XRD patterns have confirmed that F: SnO_2 powder has been possessing single phase nanocrystalline structure. SEM images (Microstructures) obtained at sintering temperature, 550°C, 650°C and 750°C have proved that a typical porous structure with many intergrain pores has been produced by this method. Since a higher temperature of 750°C can provide larger pore size of around 12nm, F: SnO_2 powder must be fabricated with this sintering temperature to replace both TCO (F: SnO_2) and TiO_2 layer in dye sensitized solar cells (DSSCs).

The FTO electrodes for using in DSSCs can be prepared by low cost spin coating method via sol-gel route. The rheological studies indicate that the excellent coating period lies between 3 and 5 days. The XRD studies indicate the polycrystalline tetragonal structure of tin oxide with preferred orientation

along the (110) plane. UV-Vis spectroscopy shows all the FTO films have good transmittance in visible region. Two point probes method shows all the prepared films have sheet resistance in kilo-ohm (kΩ) range for spin coting and ohm(Ω) range for Spray pyolysis deposition coating method. They can therefore be used as n-type electrode in fabrication of DSSCs. Since, mercurochrome, methyl blue dye and coumarin dye have higher absorbance value in both ultraviolet and visible regions, they may be used in further DSSCs' fabrication.

It was noticed that fluorine doped tin oxide powder can be used in the place of working electrodes of TCO glasses in DSSCs' fabrication. The chemical dyes can be used as sensitizer in DSSCs. The DSSCs without TCO layer has lower efficiency but higher fill factor. Therefore further study may be needed to increase cells' efficiency. The home made FTO glasses (sheet resistance = 20Ω - 50Ω) can be used to increase cells' efficiency and fill factor of the cells. To increase the stability and life time of DSSCs' the solid organic electrolyte such as agar powder may be used. To get more current, metallic mesh can be used in working electrode as current collector.